CHAPTER 4

Bulk Semiconductors for Infrared Applications

A. Burger, J.-O. Ndap, K. Chattopadhyay, and S. Morgan
Department of Physics, Center for Photonic Materials and Devices, Fisk University, Nashville, TN 37208, USA

1. Overview 239
2. Material Preparation and Basic Characterization 240
 2.1. Materials for Infrared Detection 240
 2.2. Transition Metal-Doped II-VI Compounds for Tunable Midinfrared Lasers 249
 2.3. Electro-Optic and Nonlinear Optic Materials 259
3. Material Properties Relevant for Infrared Devices 269
 3.1. Photorefractives 269
 3.2. Optical Limiters 280
 3.3. Solid-State Midinfrared Tunable Lasers 282
 3.4. Optical Parametric Oscillators (OPO) 283
 3.5. Infrared Optical Components 289
4. Conclusions 291
 References 293

1. OVERVIEW

Infrared materials are being used intensively and have penetrated almost every sector of industry, from metal cutting and welding to laser surgery in commercial and military countermeasure applications, to name a few. For example, an important class of infrared (IR) detectors, based on mercury cadmium telluride (MCT) crystals, are used for night vision and laser-guided munitions. A number of bulk compound semiconductor materials are being developed for future uses in important IR devices such as IR detectors, photorefractive devices, tunable solid-state lasers, and optical parametric oscillators. The next section explores the state-of-the-art in processing bulk IR materials. Because not all of the exciting developments could

Photodetectors and Fiber Optics, edited by H.S. Nalwa.
Copyright © 2001 by Academic Press. All rights of reproduction in any form reserved.

be cited and discussed, some of the references are intended to provide for further information.

2. MATERIAL PREPARATION AND BASIC CHARACTERIZATION

The preparation procedures of IR semiconductor materials have tremendous impact on device performance. The purity of the source materials prior to growth as well as the growth technique are determining factors affecting the quality of the crystals produced. The purification of the materials prior to growth, the growth methods, and the doping processes will be the main subjects exposed in this section.

2.1. Materials for Infrared Detection

The II–VI semiconductors are being used in numerous applications, as IR detectors, nuclear radiation detectors, LEDs, electro-optic modulators, solar cells, photorefractive devices, etc. The HgCdTe (MCT) has been the most studied II–VI material for IR detection in the 8–12 μm spectral range. However, it suffers problems of instability due to the weak bonding of Hg in the crystal network, a consequence of the addition of cadmium [1]. This effect reduces device lifetime. To solve these problems and increase device performance, HgZnTe (MZT) was then proposed. The MZT with 15% zinc has the same detection range (8–12 μm) as MCT with 22% cadmium and has comparable physical properties [2]. The incorporation of zinc stabilizes the crystal network. On the other hand, the large difference between the liquidus and the solidus in the ZnTe–HgTe phase diagram also makes difficult the growth of homogeneous crystals from the classical techniques (melt-cs and solution growth). Frequently, the same techniques have been applied to grow both materials. In other words, the MZT family has benefited from almost all the growth techniques that were previously used for MCT. These techniques include Bridgman, traveling heater method (THM), accelerated crucible rotation technique (ACRT) coupled to the Bridgman and THM techniques, and chemical vapor transport (CVT).

2.1.1. HgCdTe

In the Bridgman process, pure elements Hg, Cd, and Te are usually loaded in a clean thick wall quartz ampoule. The charge is homogenized in a vertical furnace by a slow melting, a few tens of degrees above the melting point of the MCT alloy (Fig. 4.1. [3]) and crystals are grown by a slow freezing started at one end [4–6];

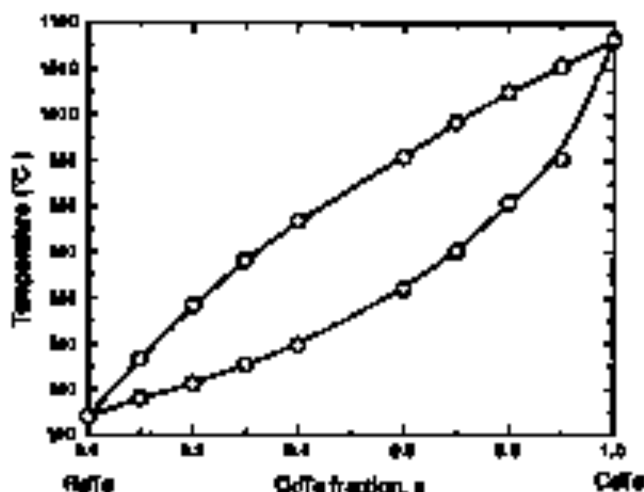

FIGURE 4.1 The HgTe-CdTe phase diagram according to the data of Szofran and Lehoczky [3].

the single crystals or large-grains ingots obtained unfortunately have large radial and axial composition variation.

THM, with tellurium as the solvent, has been more successful than the melt growth of MCT crystal insofar as the use of low-growth temperatures result in smaller radial and axial composition variations [7–11].

Solid state recrystallization (SSR) is a solid-state technique that has been used to produce large grain MCT crystals [12–16]. It unfortunately results in crystals containing a high density of dislocations and stacking faults [12,13].

The growth from the liquid suffers from the unavoidable problem of axial and/or radial compositional homogeneity, arising from two major factors: (i) the buoyancy-driven convection, always present in the melt growth performed on earth (due to thermal and solutal gradients); and (ii) and the gap between the liquidus and the solidus in the pseudobinary phase diagram (Fig. 4.2b). It was suggested that increasing the stirring in the fluid could help overcome this problem. Thus, various modifications were made to conventional liquid growth techniques. Bu *et al.* [19] applied a transverse magnetic field during vertical directional solidification. Other authors applied the ACRT during Bridgman growth [20–24] or THM growth [10,13,25–28]. The ACRT consists in accelerated/decelerated rotations in alternate directions. These modifications increased the stability of growth rates, improving the axial and radial compositional uniformity and producing larger single crystal regions of better quality. Furthermore, the ACRT was also shown to reduce the density of second-phase precipitates and to improve the control of the segregation.

The vapor growth of bulk homogeneous MCT requires a good adjustment and control of the vapor pressures of the source materials. This process is not easy, which explains the reason why this technique has not often been used in growing MCT crystals. Nevertheless, Wiedemeier and Chandra [29] applied the chemical vapor transport technique to grow bulk crystals of $Hg_{1-x}Cd_xTe$ ($x \approx 0.2$) in a closed tube, and used HgI_2 as the transport agent.

As grown from stoichiometric mixtures, bulk $Hg_{1-x}Cd_xTe$ (MCT) presents deviations from stoichiometry. It is usually mercury (Hg) deficient, due to the volatility of this element. The Hg vacancies act as acceptors, thus explaining its p-type semiconducting properties. Generally, postgrowth annealing treatments under Hg overpressure are carried out as a way to adjust the stoichiometry by this impacts the electrical properties of the crystal as required for IR detectors. The p-to-n-type conversion is of prime importance for device applications because of the high mobilities of the electrons. Numerous studies have been made on p-to-n-type conversion in MCT [13,30]. Temperatures for annealing experiments were chosen in the 260–400°C range. Because of the relatively low speed of the conversion front and the relatively small energy gap of the compound, Hall coefficient (R_H) curves as a function of temperature can present reversals of sign or dips (anomalous Hall coefficient) [31]. This suggests a competition between electrons and holes, thus compensation—the core of the sample remains p-type while the skin is converted to n-type. However, the electrons and holes concentrations, as well as their mobilities, can be measured through magneto-Hall measurements analyzed with a multiple layer model [32–35]. Electron mobilities (at 4 K) as high as 4×10^5 cm^2/Vs could be calculated [36]. The variation of these electrical properties with temperature can then be modeled [36–40]. Granger and Pelletier applied an iterative model to predict the variation with temperature of electron mobility in MCT crystals of different Cd compositions. They could accurately fit their experimental data and evaluate the concentration of ionized impurities in their crystals.

2.1.2. HgZnTe

As mentioned earlier, HgZnTe has benefited from almost all the growth techniques that were applied to the more studied HgCdTe. The growth of MZT encounters the same problem of nonuniformity of the composition as in MCT, due to the retrograde pseudobinary phase diagram (Fig. 4.2) and the wide gap between the liquidus and the solidus [41]. Moreover, the relatively slow interdiffusion between Hg and Zn in the melt [42] (about one order of magnitude slower than in the case of Hg and Cd) makes obtaining axially homogeneous ingots of reasonable length a time consuming process. During melt growth, extremely high mercury

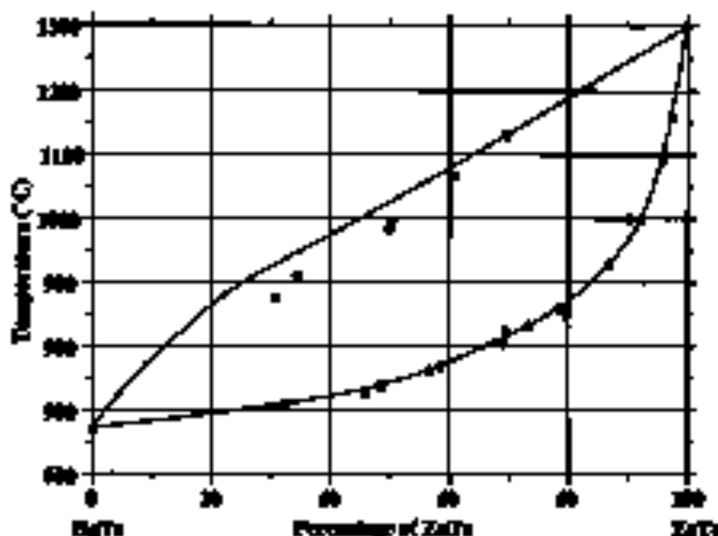

FIGURE 4.2 HgTe-ZnTe phase diagram based on data from [41].

pressures are generated in the ampoule and then thick-wall ampoules are required to reduce the risk of explosions.

Su *et al.* [43] applied the directional solidification technique to produce MZT from the melt (starting from the elements Hg, Zn, and Te) with zinc mole fractions ranging from 0.15 to 0.22. The resulting ingots presented a nonuniform axial composition profile composed of a supercooled region, a transient region, and a steady-state region. The zinc composition in the steady-state region was always found to be much lower than the initial composition. Kennedy *et al.* [44] used a modified vertical Bridgman technique and they could control the solidification interface during the growth. Nowak *et al.* [45] applied a quench recrystallization technique, and obtained ingots axially relatively homogeneous, but radially nonhomogeneous in composition. Sha *et al.* [46] applied an axial magnetic field during a directional solidification of MZT, but did not improve axial composition homogeneity.

The THM has also been applied for the growth of MZT. The growth temperatures are lower than the melting point of the compound, which reduces the risk of explosions. Tellurium was used as the solvent [2,47,28] together with a source material constituted of semicylindrical ingots of ZnTe and HgTe, cut in a way (see Fig. 4.3) that produces the needed composition along the ingot. This resulted in axially more homogeneous ingots (Fig. 4.4) with a shorter transient region (compared to those obtained from the melt); the radial composition was also more homogeneous. In order to improve the composition uniformity of THM in-

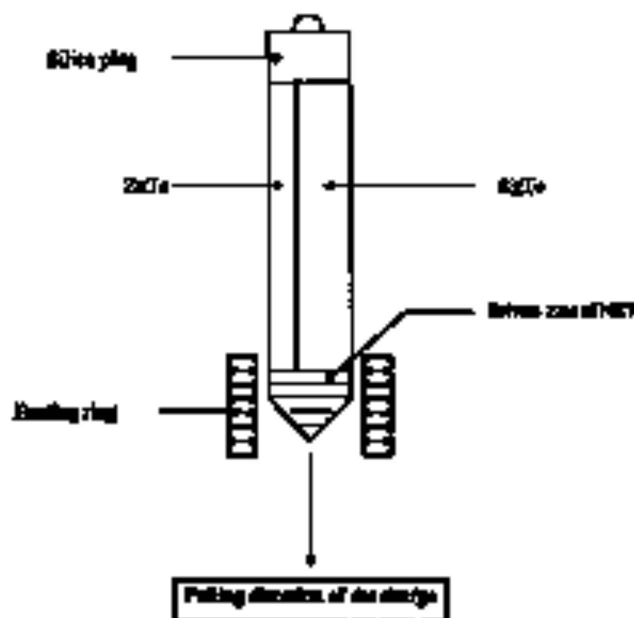

FIGURE 4.5 Simplified experimental setup for the THM growth of MZT with semicylindrical layers of HgTe and ZnTe [49].

pots, various alternative source materials have been tested [49]. This study reveals that the best results are obtained when the source material is constituted of semi-cylindrical HgTe-ZnTe or Bridgman-synthesized HgZnTe. The composition in the stationary region is close to the desired composition for the solid.

The $Hg_{1-x}Zn_xTe$ (MZT) also has been subjected to the same heat treatment conditions and characterizations as its $Hg_{1-x}Cd_xTe$ counterpart. Figure 4.5 shows the variation of the Hall coefficient and mobility as a function of temperature for a THM as-grown MZT sample of 13.54% zinc, under a 0.8 Tesla magnetic field [49]. The R_H presents a reversal of sign at 155 K, from negative to positive as the temperature drops, evidence of the electron-hole competition in the crystal.

The variation of R_H as function of the magnetic field at 77 K is shown in Figure 4.6. A sign inversion—from negative to positive—is observed at 0.12 Tesla as the magnetic field increases. A two-charge-carrier model was used to fit the experimental data in order to evaluate concentrations and mobilities at this temperature [49]. Figure 4.7 summarizes the results of analysis for different temperatures. One can see the low-temperature high mobility of electrons, evidence of a high purity material.

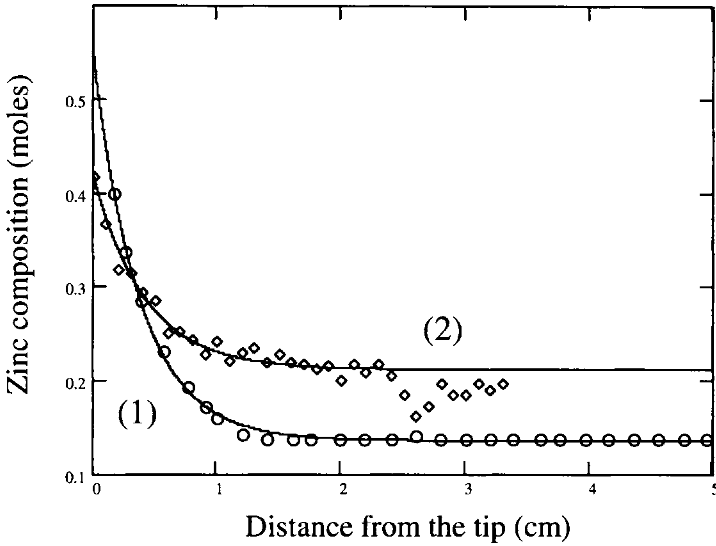

FIGURE 4.4 Axial composition profiles for MZT ingots grown by THM with semicylindrical charges of HgTe and ZnTe, with Te as solvent. The solid line corresponds to the Pfann's solution model with zinc segregation coefficients of 2.83 (1) and 2.76 (2) [48,49].

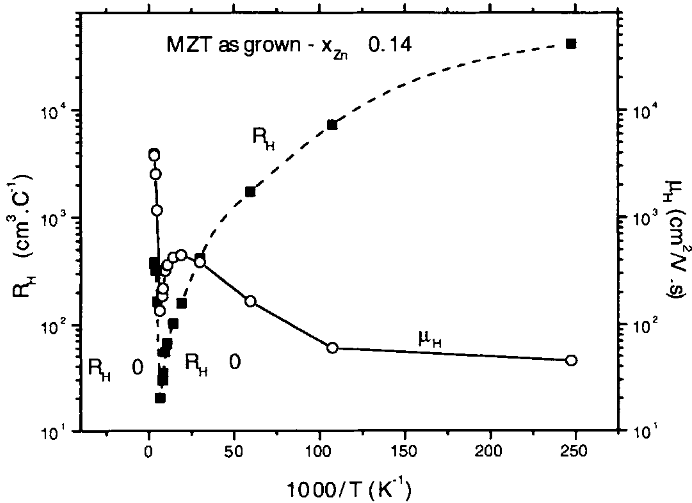

FIGURE 4.5 Temperature dependence of Hall coefficient and mobility at 0.8 Tesla for a THM as-grown $Hg_{1-x}Zn_xTe$ ($x = 0.1354$). Above 155 K, the electrons dominate the conductivity, and below that temperature the holes dominate [37].

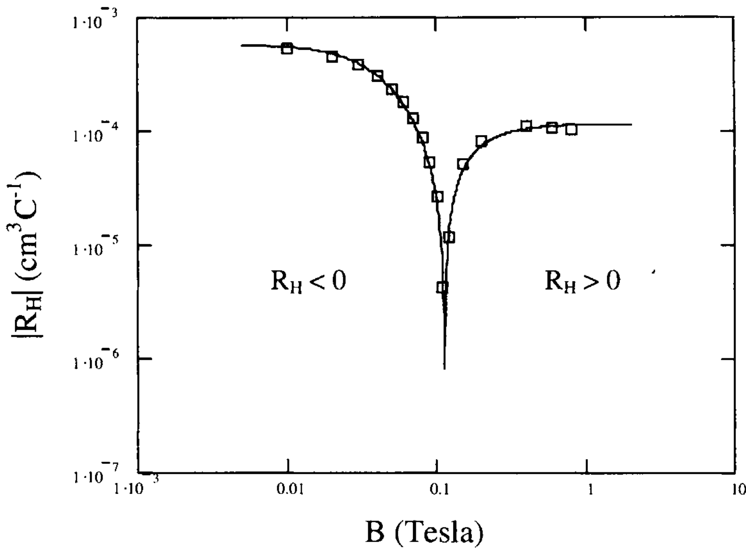

FIGURE 4.6 Magnetic field dependence of Hall coefficient at 70 K for a THM as-grown $Hg_{1-x}Zn_xTe$ ($x = 0.1354$). The solid line is the calculated curve.

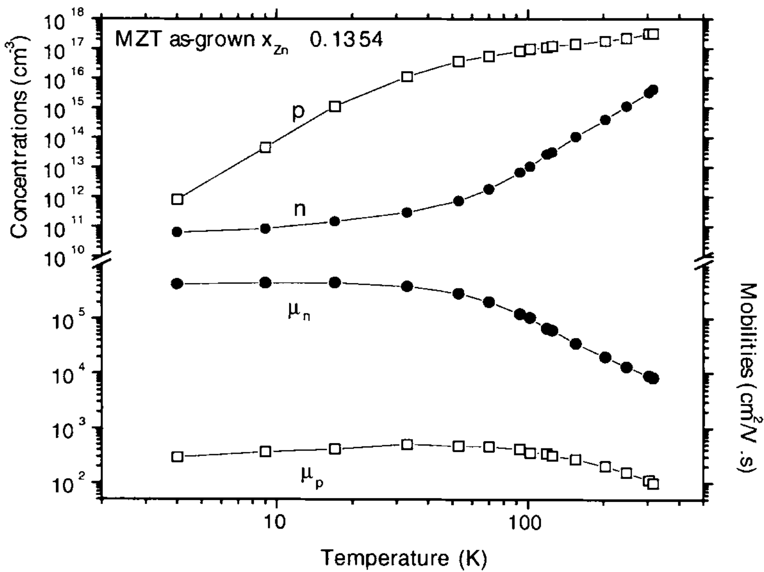

FIGURE 4.7 Concentration and mobility of electrons (n) and holes (p) versus temperature in as-grown $Hg_{1-x}Zn_xTe$ ($x = 0.1354$) by THM [49].

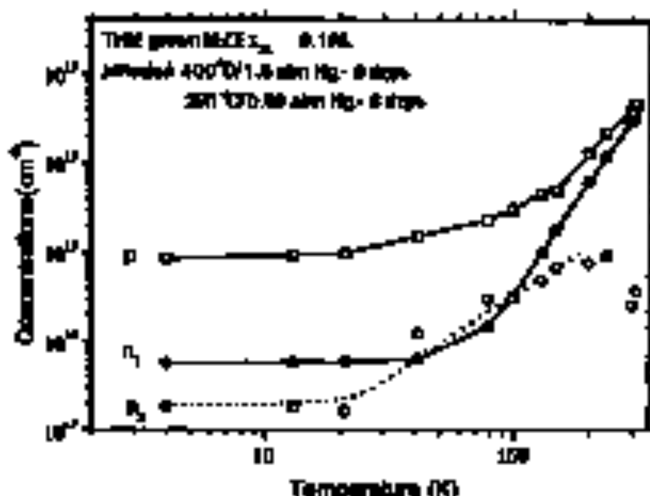

FIGURE 4.8 Concentration of electrons (n_1, n_2) and holes (p) versus temperature in a THM-grown $Hg_{1-x}Zn_xTe$ (x = 0.155) crystal annealed under Hg overpressure (400°C/1.5 atm Hg for 6 days, then 260°C/0.08 atm Hg for 6 days) [49].

Samples annealed under Hg overpressure were also studied by magnetotransport measurements with subsequent data analysis. No sign inversion of R_H was observed. However, a three-carrier model was required [49] to perfect the fit to the data points, especially at low temperature. The presence of holes in some cases was evidence of uncompleted p-n-type conversion or compensation in the annealed samples. Figures 4.8 and 4.9 show variation with temperature of the concentration and mobility of electrons ($n1$, $n2$) and holes in a MZT (x_{Zn} = 0.155) crystal annealed under Hg overpressure. One can observe that the electron-hole competition increases as the temperature is reduced. The conductivity is of n-type material because of the high mobility of electrons.

2.1.3. CdZnTe

The CdZnTe (CZT) single crystals are widely used as substrates for the growth of epitaxial layers of HgCdTe for IR detector arrays. Large crystals (7.5 cm wide, 3.5 kg) with a high purity (Cu content <2–3 ppba), low precipitate content (<10 μm in diameter and <10^4 cm^{-2} density), low dislocation density (<10^5 cm^{-2}) and high IR transmittance (higher than 60%), needed for this application, are routinely produced using the Bridgman method. Papers on CZT crystal growth improvements for IR substrate applications have been published. Copper is a particular concern when CZT is used as a substrate for MCT. One

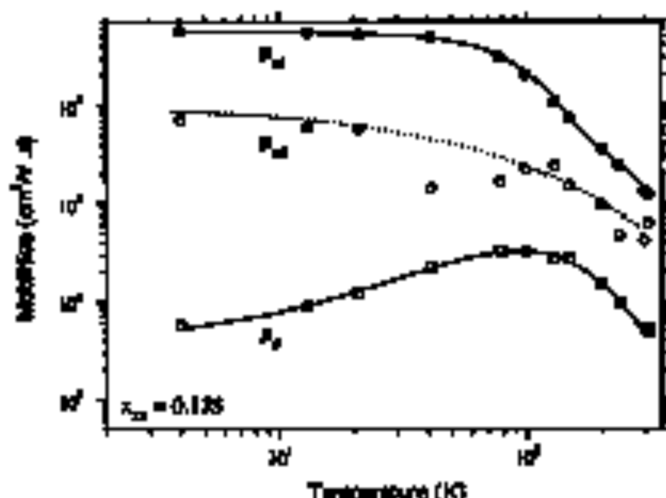

FIGURE 4.8 Mobility of electrons (μ_{n1}, μ_{n2}) and holes (μ_p) versus temperature in a THM-grown $Hg_{1-x}Zn_xTe$ ($x = 0.138$) crystal annealed under Hg overpressure (400°C/1.5 atm Hg for 6 days, then 250°C/0.09 atm Hg for 6 days) [48].

report [50] described how the concentration of Cu was reduced by using *in situ* compounding with vapor transport of the Cd into the Te (and Zn). Also reported were the results of their "boulette" experiments, which showed that growth in a slight excess of Cd greatly reduced the occurrence of precipitates (second-phase particles). Another report [51] updated the results on reducing Cu contamination and also showed that growth in a pyrolytic boron nitride crucible gave significantly lower EPD than growth in the more commonly used carbon-coated fused quartz.

In a paper by Zha *et al.* [52], $Cd_{1-x}Zn_xTe$ crystals ($x = 0.04$) were grown by the conventional vertical Bridgman technique. For characterization, they utilized a procedure developed for CdTe crystals [53]. Using the integrated area under the eutectic melting peak ≈450°C, and the value $\Delta H = 25.3$ cal/g for the enthalpy of fusion of pure Te, the concentration of Te precipitates/inclusions could be estimated. The measured broadening of the endothermic peak was probably due to impurities accumulated in Te precipitates/inclusions, which have a gettering effect. The concentration of Te precipitates/inclusions of as-grown CdZnTe crystals was then measured and a good correlation with the IR transmittance of CdZnTe wafers at a wavenumber of 1000 cm^{-1} was found. It was reported that a 0.6 wt% concentration of Te precipitates causes a reduction of the IR transmittance to values lower than 55%.

2.2. Transition Metal-Doped II–VI Compounds for Tunable Midinfrared Lasers

In the II–VI family, selenides, tellurides, and sulfides doped with transition metal ions such as Cr^{2+}, Co^{2+}, Fe^{2+}, etc., have been shown to be potential new classes of laser crystals for the mid-IR spectral region [54], and room-temperature tunable laser action has been demonstrated in ZnSe:Cr^{2+}, ZnS:Cr^{2+} [54,55], and CdMnTe:Cr^{2+} [56,57]. The host material can be a single crystal or a polycrystal. In either case, the transition metal-doped crystal is a gain medium and a saturable absorber. This section will present the growth techniques applicable for compounds in which laser action has been demonstrated, and those that have shown a broadband luminescence band in the mid-IR. The transition metal can be incorporated in the host during the growth process or by a postgrowth thermal diffusion. Basic characterization results are presented.

2.2.1. ZnSe

The ZnSe compound has been extensively investigated, mainly for its potential use in blue light emitting diodes (LEDs). Numerous growth techniques have been used to produce bulk substrates of ZnSe for homoepitaxy. Doping with transition metal has been performed either during the melt growth by introducing the dopant into the initial material [58–60] or by a postgrowth thermal diffusion of the dopant in the form of CrSe, CoSe, or FeSe [61–64].

Two methods have been used for the melt growth of undoped ZnSe. The first is the Bridgman (or gradient freezing technique), which starts from ZnSe powder in a graphite crucible, under a high pressure of inert gas (20–150 atm, to prevent noncongruent sublimation of the material) [65–70]. In this technique, the growth takes place at very high temperatures, which has the consequence of favoring the formation of the hexagonal structure (over the cubic structure), due to the 1425°C phase transition. This generates a high density of twins, voids, and inclusions in the crystals. The second method is the low pressure self-sealing technique, developed by Fitzpatrick *et al.* [71]. In this technique, the graphite crucible is sealed under a relatively low pressure of N_2 (5–7 atm) with condensed vapors of ZnSe, in order to avoid excessive losses of the initial charge. The result is that crystals obtained by this technique deviate less from stoichiometry and have a lower density of defects than those grown under the high-pressure technique [72].

Solution growth using heterosolvents such as In [73] and $PbCl_2$ [70] carried out at low temperatures in a THM configuration resulted in relatively small grain polycrystal that were contaminated with the solvent. More recently, Okano *et al.* [74],

used a ZnSe single crystal seed to grow ZnSe crystals using Zn and a mixture of Se/Te solvents. Prior to growth, their starting material was annealed under a vapor pressure of Zn for the Se/Te solvent or a vapor pressure of Se for Zn solvent in order to reduce deviation from stoichiometry.

Vapor growth has been used to produce high-quality crystals because of the low processing temperatures and the very low growth rates. The crystals are nevertheless relatively small. There are two categories of vapor growth techniques—chemical vapor transport and sublimation.

Chemical vapor transport (CVT) requires the use of a chemical transport agent such as iodine. The growth can be done in a closed tube at a temperature as low as 800°C with varying results, depending on the experimental conditions. Twin-free polycrystal ingots or needlelike crystals have been obtained in unseeded ampoules [73,75,76]. Fujiwara et al. [77] used a seed and applied the optimized conditions in Table 1 to grow large single crystals. Unfortunately, these crystals are usually contaminated with iodine. Mibella and Triboulet [78] have used water vapor as transport agent to grow pure polycrystalline ZnSe in a closed ampoule.

The chemical vapor deposition (CVD) process used industrially to produce fine grain polycrystalline window materials for IR detectors consists of gaseous H_2Se flowing over a crucible containing molten Zn (~900°C). The H_2Se (gas) reacts with Zn (gas) to produce ZnSe that deposits on a cold support.

The sublimation of ZnSe occurs at a temperature (1000–1200°C) lower than the melting point of the compound, but high enough to be in some cases close to the softening point of the quartz ampoules used. However, the sublimation growth of ZnSe is subjected less to contamination and to the problem of material stoichiometry than the former techniques. Physical vapor transport (PVT) experiments have been done in closed systems, starting from ZnSe powders or chunks, with and without seeds [79–92]. Crystals of high purity and good crystalline quality have been reported.

Sublimation growth has also been done in open systems where the ZnSe powders are heated in a stream of inert gas or H_2 under low pressure. The crystals

TABLE 1 Optimum Conditions used in [77] and [81] for the Growth of Large Single Crystals of ZnSe by CVT Using Iodine as the Transport Agent

Growth temperature	~850°
Seed orientation	(111)
Angle at the conical tip of the ampoule	<30°
Iodine concentration	1.1 mg/cm³

obtained still show some areas with high twin densities, depending on the sublimation temperatures used [93].

Solid state recrystallization (SSR) has more recently been used to grow high-quality, large single crystals of ZnSe [94,95]. The SSR is a technique that has been applied more to metals than to semiconductors. The process is different in metals, where a plastic deformation generally precedes the SSR. The SSR consists of a heat treatment that modifies the crystal structure of a fine-grain polycrystal. This transformation affects the number, the size, the shape, and the orientation of the crystallites in the solid. The migration of the grain boundaries results in the growth of some grains at the expense of others, which produces large single crystals. The SSR has the advantage of taking place at low temperatures ($0.4 \cdot T_{melt} < T_{SSR} < T_{melt} - 100°C$), and the sample remains solid during the process. Therefore, SSR-crystals are less subject to contamination.

The ZnSe needs to be doped with transition elements for use as a room temperature solid-state, mid-IR tunable laser material. Some basic characterizations are necessary in order to assess properties that give to the material its lasing potential. Absorption spectroscopy and emission spectroscopy are some of those characterizations. From the first technique, one can calculate the average concentration of doping ions in the material, and from the second, the lifetime of the excited states of the lasing ions can be obtained and laser emission can be achieved as well.

Figure 4.10 shows a room temperature spectrum of $ZnSe:Cr^{2+}$. The dominant absorption band peaking at 1.8 μm is due to the presence of chromium in the host material; moreover, it corresponds to the $^5B_2(^5T_2) \rightarrow {}^5A_1(^5E)$ optical transition of Cr^{2+} and is the pump band for laser operation. The shoulder located at 680 nm corresponds to the $^5T_2(^5D) \rightarrow {}^3T_1(^3H)$ internal transitions of Cr^{2+} [96,97]. The concentration ($N_{Cr^{2+}}$) of Cr^{2+} can be related to the peak of the absorption coefficient (α_p) at ~1.8 μm with Eq. (1) [98]. In general, the concentration of the absorbing species can be related to the absorption band through the Beer-Lambert's law, provided the absorption cross section of the absorbing species is known,

$$\alpha_p = 0.144 \times 10^{-17} N_{Cr^{2+}} \quad (1)$$

with α_p expressed in cm^{-1} and $N_{Cr^{2+}}$ in cm^{-3}.

Rablau et al. [98] reported the presence of traces of Fe^{2+} in ZnSe samples heavily doped with Cr^{2+}. The Fe^{2+} ions in ZnSe induce an absorption band that overlaps the 2–3 μm emission band of Cr^{2+}. Thus, even traces of Fe^{2+} in the host material contribute to the passive optical losses in the $ZnSe:Cr^{2+}$ lasers. These undesirable impurities should therefore be avoided by using high-purity dopants.

The emission lifetime can be calculated from a measurement of the radiative decay of the upper level ^5E, after pumping in the 1.8 μm peaking-band. Fig-

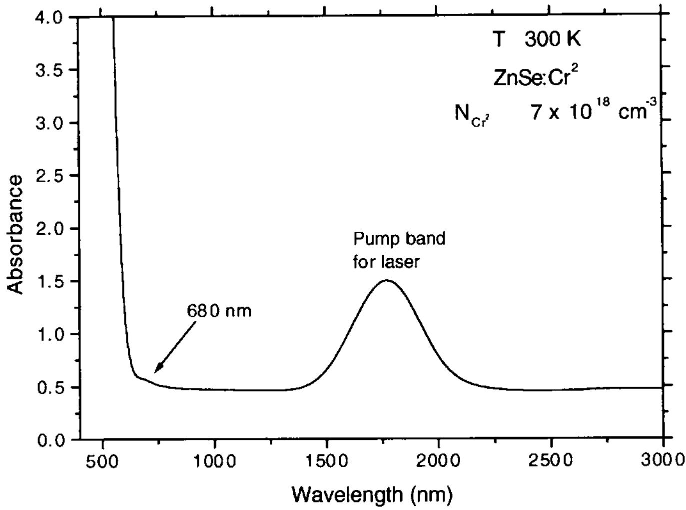

FIGURE 4.10 Absorption spectrum of $ZnSe:Cr^{2+}$, measured at 300 K.

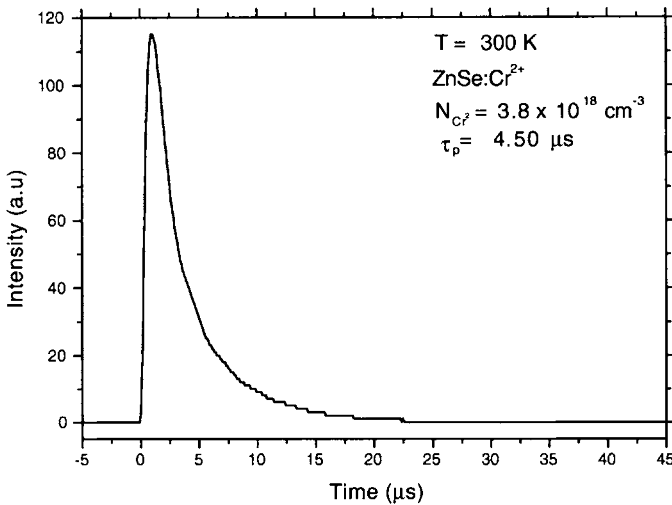

FIGURE 4.11 Luminescence decay in $ZnSe:Cr^{2+}$. The emission lifetime τ_p was calculated to be equal to 4.50 μs.

ure 4.11 shows an emission decay measured in a $ZnSe:Cr^{2+}$ doped by diffusion: a lifetime of 4.50 μs was calculated. Figure 4.12 depicts the temperature dependence of the luminescence emission lifetime in $ZnSe:Cr^{2+}$ [99]. At this moment,

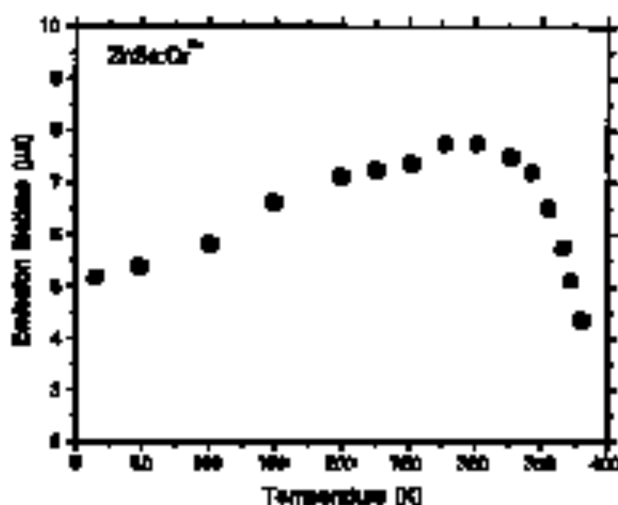

FIGURE 4.12 Emission lifetime versus temperature in chromium-doped ZnSe [99].

the gradual increase of the lifetime at low temperatures is still under investigation through application of theoretical models.

2.2.3. ZnS

Bulk ZnS crystals can be doped with transition metals in the same way as ZnSe—during the melt growth or by a postgrowth diffusion [55] applied to crystals grown from the melt or from the vapor.

The high melting point of ZnS makes its growth from the melt rather difficult. Nevertheless, a modified vertical Bridgman technique has been used by Eagle-Picher to produce ~1-cm-size ingots [100].

Chemical vapor deposition is the oldest technique applied to produce ZnS crystals. Iodine has been used as the transport agent by Du *et al.* [101] to grow polycrystals. Lewis *et al.* [102] have used H_2S, vapor of Zn and a small amount of iodine gas to produce large grain size crystals of ZnS. Suzuki *et al.* grew polycrystals using only H_2S and Zn vapor [103].

Zinc sulfide (ZnS) doped with transition elements has not been investigated as much as ZnSe for mid-IR, solid-state tunable laser applications. However, DeLoach *et al.* [55] have reported the influence of few transition elements on the spectroscopic properties of this material. The Cr^{2+} ions, for example, induce an absorption band in the 1.4–2.0-μm spectral range, with a peak at 1.7 μm. This band corresponds to the ${}^5T_2 \rightarrow {}^5E$ of Cr^{2+} ions. A broad emission band of Cr^{2+} is observed, as in ZnSe:Cr^{2+}, in the 2–3-μm spectral range. A room-temperature

(300 K) emission lifetime of 8 μs has been reported. Figure 4.13 shows the variation with temperature of the emission lifetime of the ^5E level of Cr^{2+} in ZnS. One can observe the same trends as in ZnSe:Cr^{2+}.

Table II summarizes spectroscopic properties of some transition metals in zinc chalcogenides [55].

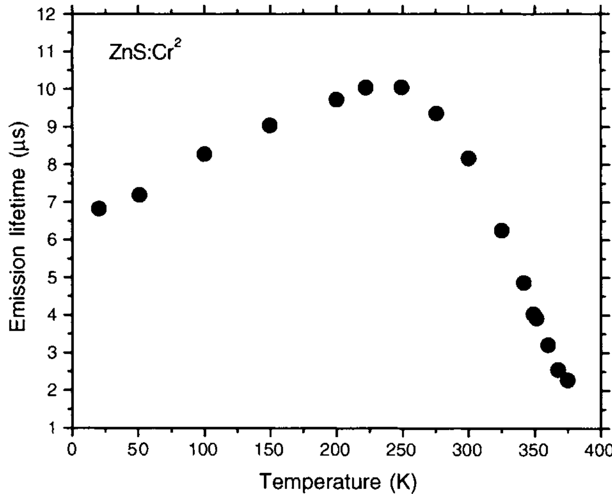

FIGURE 4.13 Emission lifetime versus temperature in chromium-doped ZnS [55].

TABLE II Spectroscopic Properties of Transition Metals in Zinc Chalcogenides [43]

	Cr^{2+} $^5E \leftrightarrow {}^5T_2$			Co^{2+} $^4T_2 \leftrightarrow {}^4A_2$			Ni^{2+} $^3T_2 \leftrightarrow {}^3T_1$	
Property	ZnSe	ZnS	ZnTe	ZnSe	ZnS	ZnTe	ZnSe	ZnS
N_{ions}[a] ($\times 10^{20}$ cm^{-3})	0.01	0.18	0.05	0.06	0.17	0.25	0.32	0.18
σ_{abs}[a] ($\times 10^{-20}$ cm^{-2})	87	52	123	7.8	5.4	4.4	8.0	14.1
σ_{emiss}[a] ($\times 10^{-20}$ cm^{-2})	92	75	188	3.7	3.5	7.1	–	–
τ_{emiss}[b] @300 K (μs)	8	8	3	290	184	50	–	–
τ_{rad}[b] @300 K (μs)	8	11	3	1173	1170	610	–	–
η_{QY}[b]	1.0	0.73	1.0	0.25	0.16	0.08	–	–

[a] N_{ions} is the concentration of doping ions; σ_{abs} and σ_{emiss} are, respectively, the absorption and the emission cross section of the corresponding ions.

[b] τ_{emiss} and τ_{rad} are, respectively, the emission and the radiative lifetime; and η_{QY} is the emission quantum yield.

2.2.3. CdSe

Chromium-doped CdSe is being investigated for its lasing potential. The Cr^{2+}:CdSe crystals can be obtained from melt, vapor, solution and also by a post-growth thermal diffusion of chromium.

The vertical Bridgman technique has been used by Schepler *et al.* to produce polycrystals that cracked due to the anisotropic thermal expansion of CdSe [104]. The use of the physical vapor transport technique to grow single crystals of CdSe was first reported by Reynolds and Czyzak [105]. The temperature gradient solution growth technique was used by Nitsu *et al.* to produce single crystals, using selenium as the solvent and CrSe as the dopant [106]. The postgrowth thermal diffusion of the dopant can be carried out on crystals obtained from melt, vapor, or solution [107–109].

The use of cadmium selenide doped with transition elements as a mid-IR, room-temperature, solid-state tunable material is under investigation. The first results reported are somewhat interesting. Continuous wavelength (cw) tunability over the 2–3 μm spectral region was demonstrated in CdSe:Cr^{2+}. Chromium ions (Cr^{2+}) in CdSe are responsible for an absorption band, peaking at 1.9 μm. Figure 4.14 shows a typical absorption spectrum of CdSe:Cr^{2+}, measured at room temperature. The concentration ($N_{Cr^{2+}}$) of Cr^{2+} can be associated to the maximum absorbance through the following simple relation, deduced from the Beer-Lambert's law (after a baseline correction):

$$A = \alpha_a N_{Cr^{2+}} d \tag{2}$$

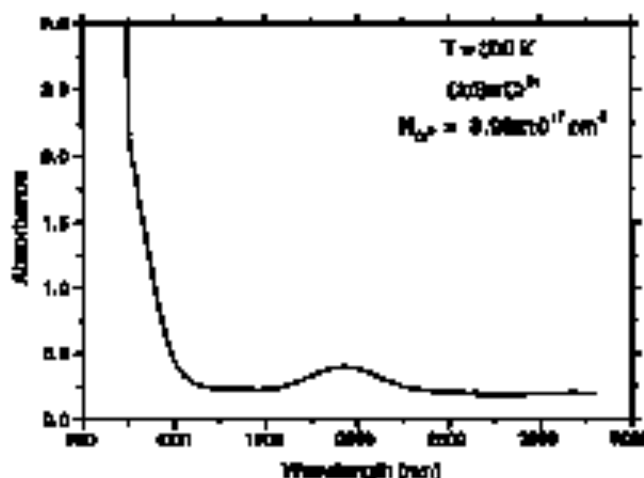

FIGURE 4.14 Absorption spectrum of CdSe:Cr^{2+}, measured at 300 K.

where σ_a is the absorption cross section of Cr^{2+} ($\sim 3 \times 10^{-18}$ cm^2 in $CdSe{:}Cr^{2+}$) and δ is the sample's thickness (expressed in cm).

2.2.4. CdMnTe

Triboulet and Didier [110] have shown that solidus and liquidus, in the pseudobinary CdTe–MnTe phase diagram, merge over a wide composition range, expressing a distribution of Mn close to one. Thus, homogeneous crystals of the same composition as the starting liquid phase can be obtained from classical normal freezing growth techniques.

Chromium has been doped in CdMnTe (at the Brimrose Corporation) during the melt-growth of the compound using a modified Bridgman method [94,111–113]. Postgrowth thermal diffusion also can be an efficient way of incorporating transition-metal ions in CdMnTe crystals obtained by the classical techniques. The Bridgman method, applied by Wu and Sladek [114] and the Brimrose Corporation [115], usually produces heavily twinned crystals. This twinning starts for manganese composition of ≈15%, and increases in density with the manganese content. The solution growth appears to be the best for producing good-quality crystals. Triboulet et al. [116] have grown $Cd_{1-x}Mn_xTe$ crystals, with $x = 0.1$–0.25 and 0.5 by THM, using Te as the solvent, at a growth temperature of 700–750°C and a pulling rate of 2–2.5 mm/day. Bridgman-grown source materials were used. Later, Azoulay et al. [117] reported high-quality single crystals (40% Mn) grown by the vertical gradient freezing solution technique, using tellurium as the solvent. These authors applied a low axial thermal gradient (3°C/cm) to the melt. The solidification was initiated by a rapid cooling and the subsequent solid annealed at above 800°C.

2.3. Electro-Optic and Nonlinear Optic Materials

2.3.1. II–VI Compounds

2.3.1.1. CdTe

Although CdTe is well known for its optoelectronic applications, mainly in radiation energy detection and in photovoltaic and photorefractive devices (in the 1.35–1.55 μm spectral region), it can also be used as a substrate for MCT epitaxy. It was demonstrated a decade ago that it also can be used as an electro-optic power limiter (EOPL) [118,119] within a 400-nm range in the near IR. Only high-resistivity crystals, with very small amounts of shallow traps, can be used for this application.

Cadmium telluride is the II-VI material on which almost all the existing crystal growth techniques have been applied (bulk and epitaxial) in order to prove crystallographic quality, as well as the size of the single crystals. The production of bulk crystal has been carried out using techniques that include the following.

(i) *Vapor growth in closed ampoules* (sublimation)—physical vapor transport (PVT) [120–126], chemical vapor transport (CVT) [127,128], give in most cases small and twinned single crystals that can be contaminated with the transport agent when using the CVT.

(ii) *Melt growth*—vertical Bridgman [129–140], horizontal Bridgman [141–143], high-pressure Bridgman (HPB) [144], and vertical gradient freezing [145,146] produce large (twinned) single crystals that unfortunately contain a relatively high concentration of impurities due to relatively high operating temperatures.

(iii) *Solution growth* has the advantage that low-growth temperatures yield less contaminated crystals. Tellurium is used as the solvent because of the higher solubility of CdTe in this element compared to cadmium. The traveling heater method (THM) is here the most widely used technique, in which the solvent zone migrates along a source material composed of a presynthesized polycrystal of CdTe or a mixture of Cd and Te (cold THM). During migration, the source material is dissolved at the "hot" interface and crystallized at the "cold" interface through the solvent zone [147–151]. The temperature gradient solution growth (TGSG) technique is also used to produce large crystals [152]. Solution growth drawbacks are the formation of a high density of Te precipitates, low growth rates, the segregation of impurities (resulting in the difficulty of achieving high and homogeneous doping levels), and poor crystalline quality due to off-stoichiometric growth conditions.

(iv) *Czochralski technique* has not been very successful. Ingots were polycrystal with small crystallites and a high density of twins [153].

(v) *The ACRT* has been combined with the Bridgman [6] and with the THM [148,149,151] in order to improve growth rates, crystal quality as well as homogeneity. Striking results have been reported.

Cadmium telluride has also been doped in order to increase the conductivity of the material for its use as substrates, decrease its conductivity via the compensation phenomenon for radiation, and incorporate deep-level impurities for electro-optic devices, phase modulators, and photorefractive devices. As-grown CdTe (from a stoichiometric charge) contains Cd vacancies (due to the high vapor pressure of this element), Te precipitates, and inclusions. To reduce their amount and compensate for Cd vacancies, the crystals are usually postannealed for a few hours under the overpressure of cadmium, which generally converts them from *p*-type to low resistivity *n*-type [138,139,151].

Very few studies of acceptor doping have been performed on CdTe, mostly because the elements Li, Na, K, Au, Cu, Sb, Ag, etc. constitute the major part of the residual impurities found in CdTe crystals grown by the classical techniques [138]. Moreover, in p-type CdTe substrates, the charge carriers have low mobilities [139,151]. Intentional doping with Ag, which substitutes for Cd, has revealed that this element has a high diffusion mobility at low temperature in CdTe [154–156].

The n-type doping during growth is usually performed with group IIIA elements such as Cl, In and Al, mostly in order to produce highly compensated high resistivity crystals [157–160]. Photorefractive applications require deep-level impurities; transition elements seem to be the convenient dopants for this purpose [139].

To assess the quality and physical properties of the materials, various characterizations are usually performed. The Hall measurements lead to quantification of the electrically active dominant impurities, as well as the mobility of the majority charge carriers. Figure 4.15 shows the temperature dependence of the majority charge carriers (electrons) in a Bridgman-grown CdTe sample. This sample was cut from a vertical Bridgman-grown ingot and annealed under a cadmium overpressure [139]. The activation energy of the electrically active impurities and the

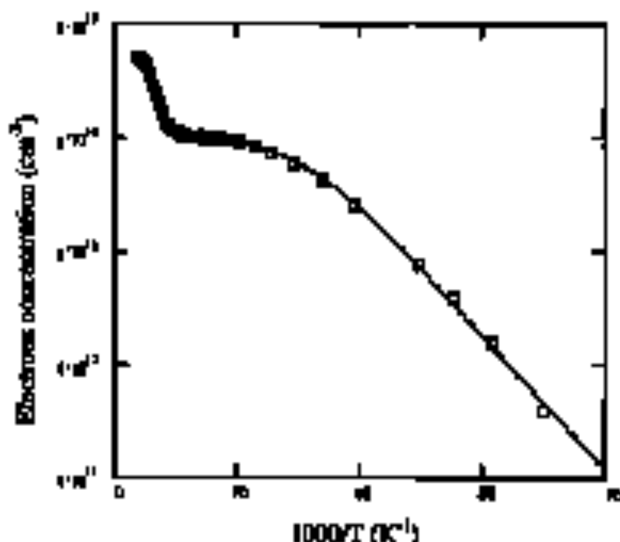

FIGURE 4.15 Hall concentration of electrons as function of temperature in a vertical Bridgman grown CdTe. The solid line is the result of the fit to the relation obtained from Eq. (3), with results summarized in Table III.

TABLE III Concentration of Impurities and Activation Energy Calculated in a Vertical Bridgman-Grown CdTe [139]

N_a (cm^{-3})	N_{d1} (cm^{-3})	N_{d2} (cm^{-3})	ϵ_{d1} (meV)	ϵ_{d2} (meV)
2.83×10^{14}	2.86×10^{14}	2.43×10^{14}	9.94	91.59

concentration of acceptors and donors can be calculated through a fit of the data to the theoretical expression of the concentration of charge carriers obtained from Eq. (3). This relation derives from the neutrality equation with two donor centers of one energy level each, and the assumption of nondegenerated parabolic energy bands:

$$N_a + n = \frac{N_{d1} \cdot N_{c1}}{n + N_{c1}} + \frac{N_{d2} \cdot N_{c2}}{n + N_{c2}} \tag{3}$$

where

$$N_{c1} = \frac{N_c}{g_1}\exp\left(-\frac{\epsilon_{d1}}{k_B T}\right), \qquad N_{c2} = \frac{N_c}{g_2}\exp\left(-\frac{\epsilon_{d2}}{k_B T}\right),$$

$$\text{with } N_c = 2\left(\frac{2\pi m_e^* k_B T}{h^2}\right)^{3/2}$$

The N_{ci} is the density of populating the donor level ϵ_{di} ($i = 1, 2$) and N_c is the effective state density in the conduction band. The N_a is the concentration of acceptors. N_{d1} and N_{d2} are the concentrations of donors 1 and 2. The m_e^* is the effective mass of electrons, k_B is the Boltzmann constant. The results obtained from the fit are summarized in Table III. These values indicate that the compensation ratio is 94% at 300 K.

The charge carrier mobility is one of the physical properties of the material that affects its application in devices. Figure 4.16 shows the variation with temperature of the mobility of electrons measured in the previous sample. The theoretical mobility was expressed according to Matthiessen's rule. Scattering on optical phonons, acoustical phonons, and ionized impurities was considered the main contributions to mobility.

2.3.1.2. ZnTe

Zinc telluride (ZnTe) is a II-VI compound that can be grown only as p-type, doped or not. Smith [161] had difficulty observing n-type conductivity in crystals heavily doped with aluminum. With a bandgap of 2.23 eV at room-temperature, bulk ZnTe single crystals have application as green light emitting devices, or epitaxial substrates for those devices. It also can be used as source material for the

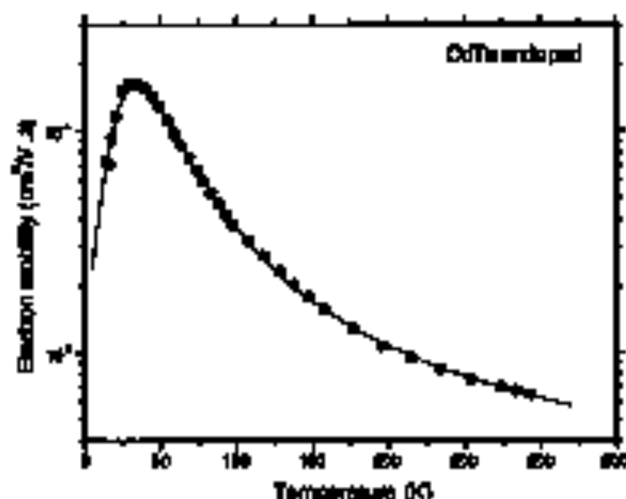

FIGURE 4.36 Hall electron mobility as function of temperature of a vertical Bridgman-grown CdTe. The solid line is the theoretical mobility defined according to Matthiessen. The concentration of ionized impurities (N_I) was calculated to be equal to 5.85×10^{14} cm^{-3}.

TABLE IV Experimental Conditions for a Vapor Growth of Undoped ZnTe [164]

Starting material	Recrystallized ZnTe
Starting material's temperature	1000 to 1025°C
Crystallization temperature	850°C $\leq T_C <$ 1000°C
Pulling rate	2.2 to 3.4 mm/day

growth of ternary alloys (HgZnTe, CdZnTe, etc.). A photorefractive response has been observed in semi-insulating ZnTe, as we report in the next paragraph. Semi-insulating crystals can be obtained by compensation of residual acceptor impurities with donors (shallow or deep levels) through doping. This will hardly reverse the conductivity to n-type.

Various techniques have been applied to grow bulky ZnTe including vapor growth [162–164]. Typical experimental conditions given by Su *et al.* [164] are presented in Table IV. The authors report good-quality crystals, free of Cu impurities. As well, growth from nonstoichiometric melts (they contain an excess of one of the elements, Zn or Te) using a modified Bridgman process [165] has been used. Table V summarizes the experimental conditions from Reference [165] and the authors reported single crystals 21 mm in diameter.

TABLE V Experimental Conditions for a Modified Bridgman Solution Growth of Undoped ZnTe [49]

Seed	Sapphire oriented (0001)
Starting material	Zn:Te = 3:7
Saturation temperature	1000°C
Temperature gradient	10°C/cm
Pulling rate	21.6 mm/day

TABLE VI Experimental Conditions for a Zone Refining Growth of ZnTe [166]

Zone's temperature	1300°C
Pulling rate	2.5–4 cm/h

TABLE VII Experimental Conditions for CTHM and THM Growth of ZnTe [49]

CTHM	
Processing temperature	950°C
Pulling rate	6 mm/day
THM	
Processing temperature	950°C
Pulling rate	3 mm/day

Third, the zone refining technique [147,166] has been used. Experimental conditions from Triboulet and Didier [166] are presented in Table VI and polycrystals were reported. Finally, the THM with a tellurium solvent was first applied on this material by Triboulet and Didier [166]. The authors reported large-grain polycrystals (2 grains per ingot 15 mm in diameter and 16-cm long) of high purity [49]. The processing temperature is usually as low as 850°C. The growth is carried out with a starting material obtained by the modified Bridgman technique or the cold THM (CTHM) in a tellurium solvent. Figure 4.17 presents the experimental setup of the CTHM and Table VII summarizes the experimental conditions for the CTHM and THM growth of ZnTe.

Hall effect measurements have been carried out to assess crystal properties [49], for example, including purity. Figure 4.18 shows the variation of the

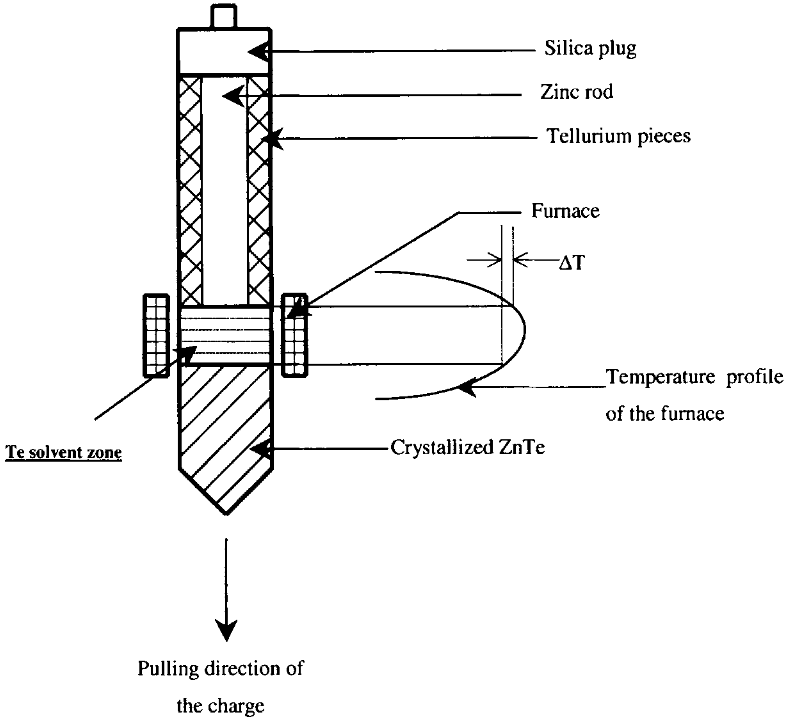

FIGURE 4.17 Experimental setup for CTHM growth of ZnTe [49].

concentration of holes as a function of the temperature for a THM-grown ZnTe. From the fit of the data using Eq. (4), it is possible to obtain the value of the activation energy ($\varepsilon_a = 126$ MeV) of the electrically active acceptor level, as well as the concentrations ($N_a = 1.53 \times 10^{15}$ cm^{-3} and $N_d = 8.49 \times 10^{14}$ cm^{-3}) of acceptors and donors, respectively. The 126-MeV activation energy corresponds to the energy of silver (Ag) in substitution for zinc [49,167] and the compensation ratio at 300 K is 55%. Hole mobility was 80 cm^2/V·s at 300 K and rose to 8000 cm^2/V·s at 45 K.

$$\frac{p \cdot (p + N_d)}{N_a - N_d - p} = \frac{N_v}{g} \exp\left(-\frac{\varepsilon_a}{k_B T}\right) \tag{4}$$

where p is the concentration of holes, g is the degeneracy factor of the acceptor energy level, k_B is the Boltzmann constant, T is the temperature and N_v is the effective state density in the valence band, $N_v = 2(\frac{2\pi m_h^* k_B T}{h^2})^{3/2}$ and m_h^* is the effective mass of the holes.

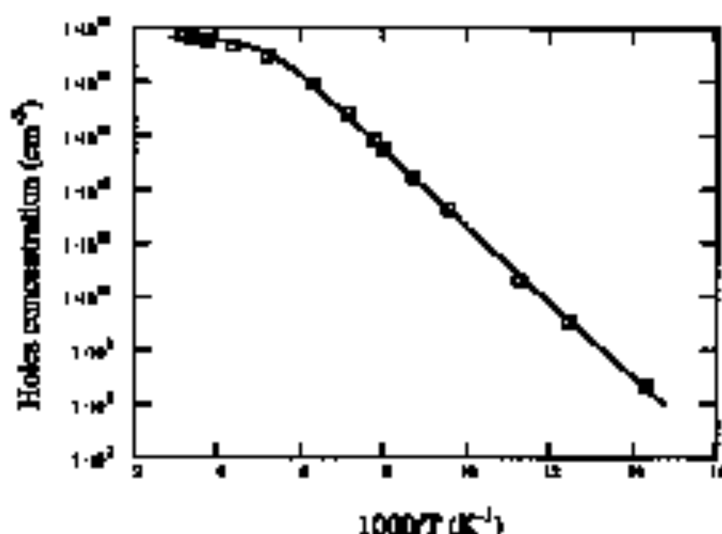

FIGURE 2.10 Hall concentration of holes as a function of 1000/T for a ZnTe sample grown by THM. The continuous line is a theoretical fit from which E_a = 126 meV, $N_a = 1.53 \times 10^{17}$ cm^{-3} and $N_d = 3.48 \times 10^{16}$ cm^{-3} [167].

2.3.2. III-V Materials

2.3.2.1. GaAs

Gallium arsenide (GaAs) crystals are now routinely grown by the liquid-encapsulated Czochralski (LEC) and liquid-encapsulated vertical gradient freeze (LE-VGF) methods to sizes >20 kg and 6 in diameter. Rudolph *et al.* [168] incorporated an arsenic (As) source in their growth chamber in order to observe the influence of the source temperature on the properties of the crystal grown by VGF. They reported the growth of single crystals for source temperatures in the range of 607–620°C, and a slight reduction of the concentration of the intrinsic deep donor defect EL2 from 1×10^{16} cm^{-3} to 6×10^{15} cm^{-3} when the source temperature was brought from 620 to 607°C. Vertical zone melting (VZM), zone leveling (in a Ga-rich melt), and zone refining techniques were also carried out for the growth of high-purity GaAs for room-temperature γ-ray detectors [169–171]. The resulting materials were reported to be electrically nonhomogeneous.

Gallium arsenide is used mostly as a substrate material for various applications, such as field effect transistors (FETs), which are useful in high-speed computers and microwave devices for wireless telecommunication, etc. It has applications in photovoltaic devices (solar cells) [172–175] and in radiation detectors [176–178]. This material can show a photoconductive response through its intrinsic deep defect EL2 [179], or when doped with chromium [180]. The EL2 defects are known to

be stoichiometric-related and they are due to As vacancies. Chromium doping is usually done by adding the dopant to the material prior to growth.

A review [181] of crystal growth of a substrate material is recommended to readers for additional information. Lower dislocation density, reduced elastic distortions, well-defined stoichiometry deviations and carbon doping levels, and precipitation control, are a few of the crystal growth issues affecting the quality of the material [182,183]. For a review of the optical properties of GaAs, the reader should consult Reference [184]. A few IR applications have been reported over the years. The GaAs single crystals are used for high-power optics in the mid-IR region due to their large nonlinear coefficient, high optical damage threshold and large coherence length (>100 μm) for second harmonic generation (SHG) in the mid-infrared region. However, GaAs cannot be birefringently phasematched. Quasiphasematching was demonstrated in GaAs [185,186] with plates aligned at Brewster's angle. Diffusion bonding of a periodic stack of GaAs (110) wafers was also reported [187,188]; the process allows a monolithic structure to be constructed that retains the excellent thermal and mechanical properties of the bulk crystal, and reduces significantly losses at the interfaces. Through optimized processing conditions, stacks of either (100)–(110)-oriented, 2-in. GaAs wafers were bonded with optical losses as low as 0.1–0.3%/interface (measured at 5.3 and 10.6 μm) [189].

2.3.2.2. InSb

The major commercial suppliers of InSb, widely used for IR detectors, use the Czochralski method [190,191]. The general problem in the growth of InSb crystal is their defects and inhomogeneities [192,193], the causes of which are still not well understood. In Czochralski growth, convection instabilities lead to striations along and transverse to the growth direction; misoriented growth and twins are also observed [194,195]. Horizontal and vertical THMs are also employed in the growth of InSb crystals [196,197], although the growth rate is extremely slow [196]. High-quality InSb crystals can also be grown with the Bridgman technique [198]. There have been various studies addressing various problems during the vertical Bridgman growth of InSb crystals from the melt, such as off-stoichiometric compositions within the binary crystal [199,200], constitutional supercooling [201], and impurity distribution in the crystal [202]. Furthermore, there is disagreement within the literature on the exact solidification point of InSb: temperatures ranging from 524 to 536°C have been reported [203].

The direct small energy gap and large carrier mobility of InSb make it a very suitable material for IR detector, filter and emitter applications [204,205] and as substrates for AlInSb devices [206,207]. Very high-quality InSb crystals, suitable for IR device applications, have been grown by the vertical Bridgman technique using an indigenous Bridgman setup with some modifications [208].

2.3.2.3. GaP

Stimulated Raman scattering (SRS) can be used to shift the emission frequency of the lasers to different spectral regions and to build laser oscillators and amplifiers that can be used extensively and effectively to control the characteristics of the laser beam. Stimulated Raman scattering has been demonstrated in various gas, liquid and ionic solid-state materials, but most practical applications involve the use of gas cells. However, a few crystals have been identified that possess the narrow, isolated and intense Raman active vibrational modes necessary for efficient scattering. In most cases, however, the stimulated Raman conversions are achieved in a passive arrangement, that is, the laser-active element and the stimulated Raman converter are different parts of the optical system. The laser crystal is kept inside the resonator and the crystal used for the stimulated Raman scattering is placed outside the resonator. Research for many years has had the goal of developing new crystals that would serve the purpose of laser action as well as that of a the host for stimulated Raman scattering.

The stimulated Raman scattering from phonons in semiconductors is very attractive because it can operate as a semiconductor FIR source at a different frequency of the pump and Stokes frequencies ω_p and ω_s. Nishizawa and Suto [209] were the first to report successful operation of a semiconductor Raman laser using a GaP crystal. Undoped GaP crystals with $n < 10^{16}$ cm^{-3}, grown by liquid-encapsulated Czochralski (LEC), were cut 10–13 mm long and the two end faces were optically polished flat and parallel to $1.6 \cdot 10^{-4}$ rad. Pumping was made by a Q-switched YAG laser operating at 1.064 μm. The details of this laser setup are given in Reference [209].

2.3.2.4. InP

The technology of semi-insulating (SI) InP substrates is becoming of great interest for a increasing number of applications in high-speed devices, such as metal-insulator-semiconductor field effect transistors (MISFETs), optoelectronics communications, optoelectronic integrated circuits (OEICs), and solar cells. The developments of InP were much later than those of GaAs and GaP because of the difficulty of growing twin-free single crystals.

The transmission loss of a quartz fiber used for optoelectronic communication has a minimum at the wavelengths of 1.3 μm and 1.55 μm [210–213]. It appears that GaInAs ternary compounds or GaInAsP quaternary compounds are well suited for lattice-mismatched epitaxial growth on InP substrates in the wavelength range from 0.9–1.6 μm.

There have been many reviews on polycrystal synthesis and single crystal growth of InP [214–219].

Several technologies have been proposed for the synthesis of InP polycrystalline material, including high-pressure horizontal Bridgman [220–222], high-

pressure gradient freezing [223–225], synthesis by solid diffusion [226], and direct synthesis [227–229]. For industrial applications there are certain requirements: (a) very high purity of polycrystals; (b) minimum indium inclusions; and (c) batch quantity as large as possible with high synthesis rate. Considering these requirements, the horizontal Bridgman technique became the most widely accepted industrial method for the synthesis of InP polycrystal material.

There is high demand for the growth of InP single crystals with high purity and low dislocation density. It has been shown from thermoelasticity models that there are two possible ways to decrease the dislocation density in InP. They are: (1) by lowering the thermal gradient in order to minimize thermal stress; and (2) increasing the critical resolved shear stress (CRSS) via a lattice-hardening mechanism.

The gradient freeze techniques, either horizontal gradient freeze (HGF) or vertical (VGF) have been widely used for the growth of III-V bulk compounds. The horizontal growth system was used to grow InP [230] in a newly designed furnace, the Mellen "electrodynamic gradient" (EDG) furnace. The key features of the system are the structure of the heating elements and the computer control of the temperature profile. The major drawback of these gradient freezing-growth methods is the poor yield of single crystals when growing along the ⟨100⟩ direction. Seeded, 50-mm-diameter InP crystals have been grown by the VGF method [231] in a pyrolytic boron nitride (PBN) crucible. In this case, the radial and axial thermal gradients were both decreased with respect to the conventional LEC process.

Although the LEC technique is advantageous for growing large-diameter single crystals with high single crystal yield, twinning is a large problem in the case of InP. A number of different methods have been adopted to reduce this twinning. One of them used B_2O_3 glass encapsulants with lower water content [232–234].

Optimization in the growth conditions, both crystal and crucible, might also help to reduce twinning. There are some reported theoretical studies on the solid/liquid interface shapes from the viewpoint of thermal balance calculations [235,236].

The high pressure LEC technique is used to grow standard-quality InP ingots. The main problems with this method is the large thermal gradients and the inhomogeneous thermal distribution. Key parameters that have been explored to minimize the LEC thermal gradient are back oxide height over the melt [237,238], thermal shield [239], gas stream and pressure [240,241], and multiheater furnaces [242].

In the case of the LEC technique, it is absolutely necessary to have a certain axial temperature gradient during growth. This induces thermal stress in the crystals, which is a main cause for the dislocations. With a normal temperature gradient of 40°C/cm, it is possible to grow dislocation-free crystals by LEC when the crystal diameter is small but if a much smaller temperature gradient is required, then vertical or horizontal Bridgman techniques are more promising for obtaining low-dislocation-density single crystals.

As mentioned, the second method to reduce dislocation density in InP is by increasing CRSS via a lattice-hardening mechanism. This is known as "impurity hardening," and can be achieved by doping with appropriate elements. The choice depends upon the device applications. Semi-insulating InP substrates are required for optoelectronics applications. For these applications the substrates must have high resistivity to isolate them. This is done by doping the InP with impurities such as Fe, Cr and Co, which form deep acceptors, or with Ti, which forms deep donors. Shallow acceptors must be intentionally added in the case of Ti doping [243,244]. For industrial purposes Fe is the dopant choice to obtain semi-insulating InP and there have been extensive studies on Fe-doped InP single crystals [245–248]. However, Co and Cr are not suitable as dopants for semi-insulating crystals because they precipitate [249]. For further improvement of semi-insulating InP, the Fe content can be reduced by using highly purified HB InP polycrystals as raw materials [250].

The reader is encouraged to go through the detailed review of InP crystal growth and characterization for a better knowledge of how to grow dislocation-free InP single crystals and also how to dope material for IR applications [251].

2.3.2.5. *GaSb*

Gallium antimonide (GaSb) has generated significant interest in its growth and characterization techniques because it has good IR detection properties. It is used mainly as a substrate material on which multiple epitaxial layers are grown for applications in optoelectronic devices. Alloys of GaSb are useful over the wide spectral range from 1.24 μm for AlGaAsSb [252] to 4.3 μm for InGaAsSb [253, 254]. Commercially-bulk GaSb crystals are grown by either the LEC or Bridgman technique. Due to the structural and compositional defects of the grown crystals, there are still limitations for the GaSb substrates to reach their full potential in solid-state electronics [255]. There has been some work done on the microgravity growth of these crystals (both doped and undoped) by the liquid encapsulated melt zone (LEMZ) technique [256] in order to better understand the defects. The ternary $Ga_{1-x}In_xSb$ is being investigated for its use in thermophotovoltaic applications [257,258].

2.3.3. Chalcopyrites

The I-III-VI_2 and II-IV-V_2 compound materials belonging to the chalcopyrite family have been synthesized from their constituents and then grown separately using the horizontal gradient freeze growth technique in a transparent furnace [259]. Difficulties in the initial experiments included the low values of the thermal conductivity, the high vapor pressure of the group VI or V element

(Se_2, Te_2, P_2 or As_2) at the melting point, cracking during cooling, and optical absorption centers in the OPO pump band. Nonwetting boat materials, such as vitreous carbon or boron nitride (which has the advantage of flexible walls), were used to prevent secondary nucleation and sticking to the evacuated quartz ampoule, and seed crystals were used to promote monocrystalline nucleation and oriented growth. Finally, and most importantly, low-temperature gradients (<5°C/cm) were used to reduce the effects of the convex solid-liquid interface in order to minimize stresses resulting from the anisotropy of the thermal expansion coefficients and suppress vapor transport. The horizontal transparent furnace was used to make it possible to control the seeding process and to monitor the growing crystal during the run. In addition, feed purification and stoichiometry control have lowered the defect-related absorption losses [260]. For $CdGeAs_2$, for example, decreasing the oxygen contamination of the starting material had a major influence on the optical transparency of the grown crystals [261].

The growth of $CdGeAs_2$ from the vapor [262] by float zoning in both Earth [263] and microgravity [264] environments and by chemical vapor transport [265], were also investigated.

The growth of $ZnGeP_2$ was attempted, with a modest degree of success, by several methods including vapor transport [266], crystallization from low melting point metals [267], and the liquid encapsulated Czochralski (LEC) technique [268]. The use of a vertical Bridgman using a ceramic jacket around the seed, careful choice of the seed orientation (to ensure minimum resolved shear stresses on the {112} cleavage planes), and flexible (boron nitride) crucibles was required to yield 20-mm-diameter, 700-mm-long, crack-free $ZnGeP_2$ crystals [269]. Effects of microprecipitation observed in this material have been attributed to a retrograde solidus on the ZnP_2 side of the pseudobinary ZnP_2-Ge phase diagram [269].

The crystal defect structure as well as the doping-incorporation processes in chalcopyrites are significantly more complicated and more difficult to study than those of the binary zincblende III-V compounds. The low-temperature photoluminescence of $ZnGeP_2$, for example, showed [270] the presence of a broad band attributed to donor-acceptor-pair recombinations, but no band-to-band recombination. The native defect characteristics for $ZnGeP_2$ and $CdGeAs_2$, as well as the dopant incorporation and their electrical properties were summarized by Baimanov et al. [271]. For $ZnGeP_2$ crystals the concentration of acceptors and donors is quite large (10^{18}–10^{19} cm^{-3}) while the free carrier concentration (p-type only) at RT is in the range of 10^{12}–10^{14} cm^{-3}. For $CdGeAs_2$, the range is narrower, 10^{16}–10^{17} cm^{-3}, indicating in both cases the presence of compensating defects. For $CdGeAs_2$, for example, doping with Ga and Cu produces p-type crystals while doping with In and Te causes n-type crystals.

Several methods have been employed to improve the quality of the grown crystals. For $AgGa_xIn_{1-x}Se_2$ grown by the directional crystallization method, an an-

annealing process for 20 days at 10–20 K below the melting point was found to be useful [272]. Postgrowth vacuum annealing was found useful for decreasing the p-type conductivity and increasing the optical transmission of $AgGaTe_2$ crystals, while annealing in Te decreased the optical transmission [273]. In their study of $ZnGeP_2$ annealing, Schunemann and Pollak [274] noticed a correlation between the effect of annealing and the initial composition of the crystal, with the most remarkable reduction in absorption occurring in near-stoichiometric crystals. Unfortunately, the homogeneity range of $ZnGeP_2$ has not been studied experimentally and its width remains unknown. Long-term (300 h), low-temperature annealing of as-grown $ZnGeP_2$ was reported [275] to lead to improvements in the optical absorption that did not correlate with the sample size nor the vapor composition in the ampoule. This led the authors to conclude that interaction between pre-existing point defects, rather than the diffusion of external species, was involved in transmission improvement.

For $CdGeAs_2$, annealing under As overpressure at 520°C produces p-type material while annealing under Cd overpressure at 400°C was shown to produce n-type material. The temperatures for the As and Cd reservoirs were 510 and 390°C, respectively [271]. Irradiation with high-energy (1–4.5 MeV) electrons [276–278] and γ-rays (^{60}Co) [278,279] increased the resistivity and reduced the optical absorption near the bandedge for as-grown $ZnGeP_2$. The primary defect produced during irradiation is considered to be the Frenkel pair (vacancy plus interstitial complex). Such a defect requires threshold energy of 14 to 35 eV, depending on the material [280]. The irradiation-induced defects were attributed to compensation of the native defects (in particular the V_{Zn}), which were identified by EPR studies [281].

3. MATERIAL PROPERTIES RELEVANT FOR INFRARED DEVICES

This section will review the basic material properties relevant for IR use of bulk semiconductor crystals in photorefractive devices, optical limiters, MIR lasers and optical parametric oscillators.

3.1. PHOTOREFRACTIVES

3.1.1. Basic Principle and Background

The photorefractive effect, that is, a refractive index change induced by a light field, was first discovered [282] as an unwanted "optical damage" in $LiNbO_3$ and $LiTaO_3$ crystals that were used for nonlinear optical purposes [283], such as

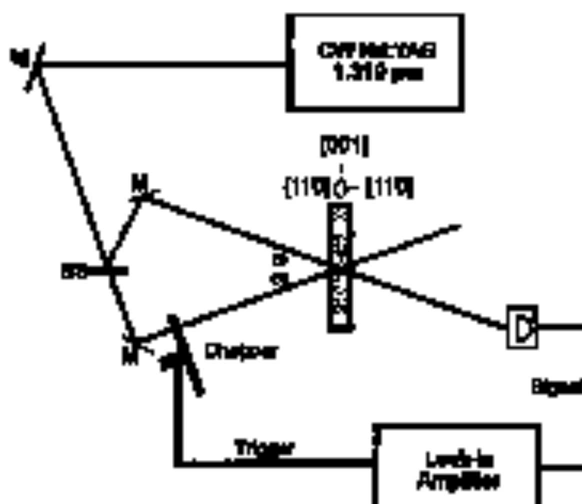

FIGURE 4.19 Experimental setup for photorefractive two-beam coupling.

second-harmonic generation. This photorefractive effect can also be explained as a real-time holographic optical nonlinearity that is effective for low power lasers over a wide range of wavelengths.

If two mutually coherent laser beams are incident on a photorefractive crystal as shown in Figure 4.19, the coherence between the two beams will produce an interference pattern with dark and bright areas (fringes).

Charge carriers are preferentially excited in the bright fringes while a smaller number of carriers are generated in the darker fringes. Thus, the interference process is periodic and will result in a periodic charge distribution with the same spatial period and phase as the beams. Due to this carrier concentration gradient, the excited carriers drift and diffuse into areas where the concentration is lower. During this process, they may temporarily recombine to trap centers and subsequently be re-excited (as long as the light is of sufficient intensity). In this way, a space charge builds up inside the crystal in phase with the interference pattern. The electric field of this space charge acts through the linear electro-optic effect to form a volume holographic refractive index grating in real time, that is, the development of this grating occurs with a time constant of the order of the response time of the photorefractive crystal.

It is important to note that the electric field is spatially shifted by 90° with respect to the interference pattern, and the refractive index grating is also shifted by 90°. This shift is possible because of the dependence of the refractive index perturbation on the direction of the electric field, not just on its magnitude. The direction of the shift is governed by the sign of the electro-optic coefficient and

crystal orientation. Due to shifting of the grating with respect to incident optical interference pattern, the beam coupling results in energy transfer from one beam to the other.

By chopping the pump beam and monitoring the signal beam, the photorefractive gain can be measured. The ratio of the modulation of the signal-beam ΔI_s with the pump beam to the signal beam I_s without pump beam is called photorefractive gain. The photorefractive gain Γ may be found using the following equation

$$\frac{\Delta I_s}{I_s} = \frac{\exp(\Gamma L) - 1}{1 + \beta \exp(\Gamma L)} \tag{5}$$

where L is the overlap length of the beams and β is the intensity ratio of the signal beam to pump beam. Equation (5) could be solved for Γ to give the relation

$$\Gamma = \frac{1}{L} \ln\left[\frac{\Delta I_s/I_s + 1}{1 - \beta \Delta I_s/I_s}\right] \tag{6}$$

The gain coefficient Γ also could be estimated by using a simplified model given by Kukhtarev and others [283]:

$$\Gamma = \frac{2\pi (n_0^3 r_{eff})}{\lambda \cos\theta} \left(\frac{k_B T}{e}\right) \frac{k_g}{1 + (k_g^2/k_D^2)} \xi_0 \tag{7}$$

where ξ_0 is the electron-hole competition factor, k_D is the inverse of the Debye screening length, r_{eff} is the effective electro-optic coefficient and n_0 is the linear refractive index. The choice of the components of r_{eff} depends on crystal point symmetry group, sample orientation, and beam polarization. For a one-level model, $k_D^2 = (e^2/\varepsilon k_B T) N_{eff}$, where N_{eff} is the effective trap density, ε is the dielectric constant, and k_B is the Boltzmann constant. The value of grating wave vector is given by $k_g = 2k \sin\theta$ where 2θ is the angle between the two crossed beams. An important intrinsic property affecting the photorefractive response of a given material is thus the product $n_0^3 r_{eff}$, where n_0 is the linear refractive index and r_{eff} is the appropriate component of the electro-optic coefficient. The choice of component depends on the crystal point group, sample orientation, and beam polarization.

The relationship between materials properties and photorefractive response can be illustrated using a simple band transport model with a single defect [285] (as shown in Fig. 4.20). The total defect concentration is N_T, the concentration of ionized defects is N_0, and the concentration of neutral defects is $(N_T - N_0)$. For simplicity, such a case would be when the crystal contains N_A acceptors and N_D donors with $N_A \ll N_D$, with the assumption that all the acceptors are completely filled with electrons that have fallen from donor levels and these filled acceptors cannot be ionized by thermal and optical means. Thermal and optical excitation of electrons is then possible from the $N_D - N_A$ neutral donor levels. There are

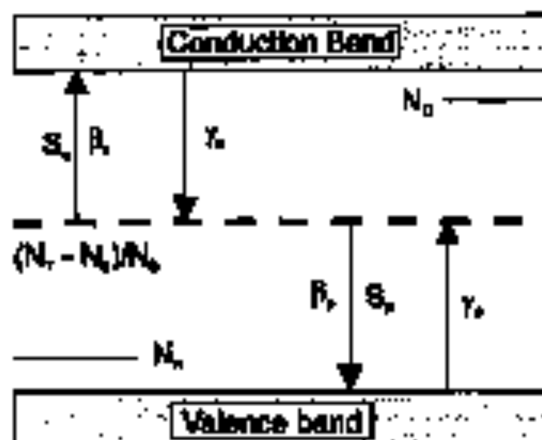

FIGURE 4.20 Energy diagram of a semiconductor assuming single deep-level defects.

the actual levels that give rise to the photorefractive effect and the emission from these levels is governed by the rate of ionization β and its cross section S, while the recombination coefficients are given by γ_n and γ_p. In a two-beam coupling experiment, with no applied field and incident intensity I_0, the space-charge field is described by

$$E_1 = -i\frac{k_B T}{e}\frac{k}{1+(k^2/k_0^2)}\xi_0 \tag{8}$$

Where $i = (-1)^{1/2}$, k is the magnitude of the grating wavevector, $k_0 = [(e^2/\varepsilon k_B T)N_{eff}]^{1/2}$ is the inverse of the Debye screening length. $N_{eff} = N_0/N_T\,(N_T - N_0)$ is the effective trap density, and ξ_0 is the electron-hole competition factor.

The photorefractive response is also affected by several intrinsic, or defect-related parameters. Equation (8) illustrates the importance of the electron-hole competition factor ξ_0. This coefficient varies between -1 (holes as majority carriers) and $+1$ (electrons as majority carriers). The gain is maximum for the monopolar case, that is, $|\xi_0| = 1$, and is zero in the case of exact compensation. Because the electron mobility μ_e is much larger than the hole mobility μ_h, one expects a faster photorefractive response for electrons as majority carriers. Also important for high photorefractive gains is the effective trap density N_{eff}, which gives the maximum number of charges that can be redistributed and therefore determines the magnitude of the space charge field that can be induced. Doping with transition metal ions, such as vanadium, has generally been used as a means of increasing the effective trap density in II-VI and III-V semiconductors. It should also be possible to improve the performance of II-VI materials, for example, as

specific wavelengths by alloying (such as in the $Zn_xCd_{1-x}Te$ system). By varying x, one can tune the bandgap to take advantage of the increased electro-optic coefficient near resonance [284].

In a one carrier model, Γ can be rewritten as a function of I_d, the equivalent dark irradiance, defined as the irradiance at which the dark conductivity is equal to the photoconductivity, or $\sigma_d = \sigma_{ph}$. The saturated gain coefficient, Γ_m, is the value of Γ for $I \gg I_d$. Therefore, for good photorefractive performance, the photoconductivity σ_{ph} should be greater than the dark conductivity σ_d. This condition provides a measure of the minimum irradiance at which a photorefractive crystal can be used.

$$\Gamma(I) = \frac{\Gamma_m}{1 + \frac{I_d}{I}} \tag{9}$$

With further approximations, $\beta \ll SI_0$, $n_A \ll N_A$, and $n_0 \ll N_T$, the time response of the photorefractive grating can be described by

$$\tau = \tau_{di} \frac{1 + E_D/E_M}{1 + E_D/E_q} \tag{10}$$

where

$$\tau_{di} = \frac{\epsilon_{DC}}{4\pi e \mu n_{e0}}, \qquad E_D = \frac{k k_B T}{e}, \qquad E_M = \frac{\gamma N_A}{k\mu}, \qquad E_q = \frac{4\pi e}{\epsilon_{DC} k} N_{eff} \tag{11}$$

and n_{e0} is the mean electron density, N_A is the concentration of electrons bound to acceptor impurities, and ϵ_{DC} is the dc dielectric constant. These equations show the relationship between the electron (hole) mobilities and the response time of the photorefractive grating. From these equations it can be seen that for applications requiring fast writing and erasure of photorefractive gratings, it is important to use a material with high carrier mobilities. A response time on the order of 10 μs can be anticipated in II-VI and III-V compounds [286]. Slow components in both the build-up and decay of gratings have also been related to transient trapping to shallow levels [284,287]. In order to understand this aspect of the photorefractive response, further research is necessary to characterize the shallow levels in groups II-VI and III-V semiconductors.

3.1.1. Semiconductor Photorefractive Materials

3.1.1.1. *Requirements for a Photorefractive Material*

A good photorefractive material should contain enough trap levels that can create the space-charge field necessary to modulate the refractive index through the Pockels' effect. It should not have an inversion center of symmetry, a condition

necessary for the previous effect to take place. It should have a high electro-optic coefficient. The material should be semi-insulating in order to allow the application of relatively high electric fields. The practical resistivities should be higher than 10^7 Ω cm. For short response times under illumination, the charge carrier's mobilities should be high enough. The material should be transparent to the optical spectral range considered for its applications, with a high photoconductivity. It should be of good purity, because too many residual impurities can reduce the solubility of the dopant in the host and may scatter and absorb the incident light beams. Materials of good structural quality are required for good modulation of the space-charge field; they should be free of precipitates.

The semiconductor photorefractive materials have several other features that make them particularly attractive for possible devices. Some of these features are listed here [288]:

- Photorefractive materials can be highly efficient at power levels obtained using CW lasers. Image amplification with a gain of 4000 [289] and degenerate four-wave mixing with a reflectivity of 2000% [290] have been demonstrated.
- The characteristic phase shift between the writing intensity pattern and the induced space-charge field leads to energy exchange between the two writing beams, amplified scattered light (beam fanning), and self-pumped oscillators and conjugators.
- In optimized bulk photorefractive materials, the required energy to write a grating can approach that of photographic emulsions (50 μJ/cm^2), with even lower values of write energy measured in photorefractive multiple quantum wells.
- The response time of most bulk photorefractive materials varies inversely with intensity. Gratings can be written with submillisecond response times at CW power levels and with nanosecond response times using nanosecond pulsed lasers. Most materials have a useful response with picosecond lasers.
- The high dark resistivity of photorefractive materials allows the storage of holograms for time periods up to a year in the dark.

Due to these features these materials have potential device applications in optical signal processing and related areas [291,292]. These applications include, among others, reversible holographic storage [293], tracking filters [294], optical interconnects [295], and neural nets [296].

The choice of the dopant depends on the way in which it induces a deep level in the forbidden band of the material. The dopant should be soluble in the host, because increasing its concentration strengthens the space-charge field and the contrast of the refractive indexes' network.

The gain (Γ) characterizes the quality of the photorefractivity of a material. It is a function of the parameter ξ_0, electron–hole competition factor, which depends on the crystal growth conditions. The gain is maximum when only one type of charge carrier induces the photorefractivity effect. Consequently, the choices of crystal growth techniques as well as the growth parameters affect the photorefractive properties.

Investigations on photorefractive effects have been carried out on various types of materials. Most work has been on oxides. Ferroelectric oxides ($LiNbO_3$, $LiTaO_3$, $KNbO_3$, etc.) doped with Fe have the highest electro-optic coefficients, but rather low sensitivities, which have somewhat reduced their use in practical devices. Sillenites ($Bi_{12}SiO_{20}$, $Bi_{12}GeO_{20}$, $Bi_{12}TiO_{20}$), ceramics ($Pb_{1-x}La_xZr_yTi_zO_3$), and emulsions have also been studied. Polymers (PVF_2) are morphologically flexible so that they can be used in deformed-mirror adaptive systems. Cerium-doped rare earths (Ce) [297] also have shown interesting photorefractive properties.

Semiconductors have only recently interested investigators. The good quality of available crystals induces large carrier mobilities that result in large diffusion lengths, leading to fast response times. Particular attention has been focused mostly on III-V and II-VI compounds, due to the need for photorefractive materials, compatible with semiconductor lasers that operate in the near-IR. However, Mizutani *et al.* [298] have reported a photorefractive effect in $CdGa_2S_4$ (chalcopyrite) at 0.633 μm in the visible. Although semiconductors have smaller electro-optic coefficients than those of oxides, their resulting sensitivities are of the same order because of their small dielectric constants [299].

3.1.2.2. *Bulk Semiconductor Photorefractive Materials in the Infrared*

Among the III-V compounds, photorefractivity has been mostly studied in GaAs and InP because they could be easily grown in a bulk semi-insulating form. However, other binary materials of this group also have been investigated. In the II-VI family, CdTe and ZnTe appear to be the most interesting because they present higher electro-optic coefficients in the IR than the most studied III-Vs (see Table VIII). Their only problem is the availability of high-quality crystals.

GaAs. In 1984 Glass *et al.* [180] predicted a photorefractive response in GaAs, when doped with chromium, as far into the IR as 1.8 μm, based on absorbance measurements. This effect was subsequently measured from the near-band edge at 931 nm to 1.3 μm [300,301]. Gain coefficients as large as 0.4 cm^{-1} were measured under conditions of a zero externally applied electric field, and as large as 14 cm^{-1} with applied electric fields and near-resonant effects. The application of electric fields can result in spatial nonuniformities, which are due to mobile domains of high electric fields in the crystal. Rajbenbach [302] confirmed

TABLE VIII Optical and Electro-Optical Properties at 300 K of Some Photorefractive Materials

Material	E_g[a] (eV)	Crystal symmetry	σ_d[a] ($\Omega^{-1}\cdot cm^{-1}$)	n_o[a] (at λ μm)	r_{ij}[a] (pm/V) (at λ μm)	$n_o^3 \cdot r_{ij}$ (pm/V)	ε[a]	μ[a] (300 K) (cm^2/Vs) *(undoped)* Electrons	Holes
II-VI materials									
CdTe	1.56	$\bar{4}3$ m	$<10^{-10}$ *(V doped)*	2.82 (1.30)	5.79 (1.32)	130	9.4	1050	100
ZnTe	2.27	$\bar{4}3$ m	$<10^{-9}$ *(compensated)*	2.7 (2.06)	3.2 (3.39)				
				2.9 (0.70)	4.3 (0.63)	105	10.1	/	100
				3.1 (0.57)	4.45 (0.59)	133			
CdSe	1.70	6 mm	$<10^{-12}$ *(compensated)*	2.5 (3.39)	1.8 (3.39)	28	10.65	800	/
CdS	2.47	6 mm	$<10^{-10}$ *(compensated)*	2.5 (0.63)	1.1 (0.63)	17	10.33	350	/
ZnSe	2.68	$\bar{4}3$ m	$<10^{-12}$	2.66 (0.55)	2.0 (0.55)	38	9.1	400	
III-V materials									
GaAs	1.42	$\bar{4}3$ m	$<10^{-10}$	3.5 (1.02)	1.33 (1.06)	57	13.2	8500	400
InP	1.35	$\bar{4}3$ m	$<10^{-8}$	3.29 (1.06)	1.45 (1.06)	52	12.6	4600	150
GaP	2.26	$\bar{4}3$ m	$<10^{-8}$	3.45 (0.54)	1.07 (0.56)	44	12	110	75

[a] E_g is the energy bandgap, σ_d is the dark conductivity, n_o is the ordinary refractive index, r_{ij} is the linear electro-optic coefficient ($ij = 41$ and 33, respectively, for the $\bar{4}3$ m group materials and σ-mm group materials), ε is the dielectric constant, and μ is the charge carriers' mobility given for undoped materials) [37,49,119,213,411–414]. Note that σ_d and μ vary depending on the growth technique, growth conditions, and purity of the materials.

these domains to negative differential resistivity arising from field-enhanced capture of charge carriers by deep level traps, which can be other than the dopant (Cr). Low-frequency-current oscillations observed in semi-insulating GaAs (also in InP) are believed to be caused by these propagating domains. Investigations related to these domains have been carried out for various purposes—to find a way to control their formation [299,303] as well as the new method of extracting information on deep levels [304]. Billing *et al.* [299] report that the formation of domains could be controlled by optical means. The experimentally determined optimum electric field that can be applied in GaAs:Cr for photorefractive actions without inducing field nonuniformities is ≈4 kV/cm [303].

InP. Indium phosphide crystals can give a photorefractive response when they are doped with either iron (Fe) or titanium (Ti). This was first demonstrated in 1984 by Glass *et al.* [180] and Nolte *et al.* in 1989 [306]. Photorefractivity has been observed in the spectral range going from 970 nm to 1.32 μm [307,308]. A gain of 0.27 cm^{-1} was measured at 1.32 μm in InP:Fe [308], without any applied electric field. This gain could rise up to 30 cm^{-1} at 980 nm under applied electric fields. Field domains similar to those reported in GaAs have also been observed in InP:Fe, but at temperatures lower than ≈77 K [309]. As the temperature increases, the deep-level traps are more and more depopulated, thus weakening the electric field in the domains, so that at 300 K, the high-field domain related trapping process is completely absent. However, another mechanism favoring the build-up of high-field domains has been reported at room temperature in InP:Fe, when used in a double pumped phase-conjugate arrangement [310–312]. In the double phase conjugate mirror (DPCM) configuration, the field-domains are due to a negative differential resistivity caused by the sudden increase of the intensity fringe contrast inside the material as soon as the DPCM achieves threshold. Wolffer and Gravey [311] eliminated the effects of these domains by using an alternating lens together with the DPCM. Ozkul *et al.* [313] reported that the photorefractive effect in InP:Fe could be reduced by the indirect transitions involving the excited state of Fe^{2+}, when the majority photocarriers are holes at room temperature.

GaP. Gallium phosphide (GaP) has not been investigated for its photorefractive response as much as GaAs and InP. This is due mainly to the difficulty in growing semi-insulating crystals. The particularly wide bandgap of this material permits photorefractive activity in the visible. Kuroda *et al.* [314] reported a gain of 0.33 cm^{-1} at 633 nm in the visible. However, absorption measurements indicate that photorefractivity in this material should extend out to 1 μm in the near IR.

CdTe. Photorefractivity was first reported in doped CdTe by Bylsma *et al.* in 1987 [284]. These authors doped CdTe, grown using the Bridgman method, with

vanadium concentrations ranging from 5×10^{17} to 7×10^{19} cm^{-3}. Dark resistivity values were reported to be $>10^{8}$ Ω-cm, and effective trap densities were on the order of 10^{15} cm^{-3}. Beam coupling and four-wave mixing experiments at 1.06 μm yielded a Γ of ~0.7 cm^{-1}, which is more than twice that of GaAs. Since 1987, there have been a number of other studies on photorefractive CdTe:V [290,315–321]. Vanadium doping concentrations have ranged from approximately 10^{17} to 10^{19} cm^{-3} and resistivity values from around 10^{5} to 10^{10} Ω-cm. In spite of the wide range of doping concentrations, the reported values of effective trap density N_{eff} vary only by a factor of ≈2 (8×10^{14} to 1.5×10^{15} cm^{-3}). This would imply that the trap density in CdTe:V is determined by other defects in the crystals [284]. In addition to photorefractivity measurements, techniques that have been applied to CdTe:V include optical absorption [320,321,323], photoconductivity photoluminescence [321], EPR [315,321], photoinduced current transient spectroscopy [322], and DLTS [248].

Measurements of photorefractive gain in CdTe:V with zero applied field have yielded values of 0.9 cm^{-1} [322], 0.7 cm^{-1} [284,322] and 0.08 cm^{-1} [318] at 1.06 μm, 0.26 cm^{-1} [319] and 0.08 cm^{-1} [318] at 1.3 μm, and 0.26 cm^{-1} [318], at 1.5 μm. Photorefractive gains with an applied field are higher, with values of 3.5 cm^{-1} [316] and >10 cm^{-1} [286] being reported at 1.06 and 1.3 μm, respectively. Reported values of both the magnitude and sign of the electron-hole competition factor differ significantly. Although there is agreement that electrons are the majority carriers at 1.06 μm [316,318,321], the situation at other wavelengths appears to be sample dependent. Schwartz *et al.* [321] report that electrons are the majority carriers at 1.3 and 1.5 μm, while Roosen, Moisan and co-workers [318,320] determined that the majority carriers were holes for their samples. Bylsma *et al.* [316] and Launay *et al.* [317] measured gains near zero at 1.5 μm, which implies almost exact compensation.

ZnTe. Zinc telluride (ZnTe) has a high electro-optic coefficient, suggesting that gain coefficients comparable with those of CdTe may be obtained if high trap densities could be introduced in the material. Unfortunately, this material has not been very attractive for photorefractive applications. This fact is probably due to the presence of multiple defect levels in the available crystals. These multiple defects induce the electron-hole competition, which causes measured low gains. Ziari *et al.* [288] reported photorefractivity in ZnTe:V in the 0.63–1.32 μm spectral wavelength. They measured grating formation time of 15 μs at 0.63 μm with an intensity of 4.7 W/cm^{2}, value comparable to GaAs at 1.06 μm, but shorter (faster grating formation) than photorefractive cubic and ferroelectric oxides. They reported two beam coupling (TBC) gains of 0.43 and 0.12 cm^{-1} at 633 and 830 nm, respectively [162].

Ternary alloys: $Cd_{1-x}Zn_xTe$, $Cd_{1-x}Mn_xTe$ and $CdS_{1-x}Se_x$. Ternary solid solution alloys show a particular attraction because varying the mole fraction (x) in the 0–1 range moves the value of their bandgap between the values of the two binary components of the alloy. This can have the advantage of providing a tunable photorefractive-sensitive wavelength range [319,162] and also a better material quality.

There have been few reports on photorefractive properties of $Cd_{1-x}Zn_xTe$. Ziari *et al.* [162] reported TBC gains as high as 0.45 cm^{-1} at 1.06 μm, with no applied electric field, in a sample with a 10% zinc composition. Studies have been done on samples with 1- and 4% zinc [163,324–326]. Figure 4.21 shows the TBC gain as a function of the pump beam intensity at 1.32 μm, with no applied electric field. A saturated gain of 0.398 cm^{-1} and a dark irradiance of 0.06 mW/cm^2 could be calculated theoretically. Under no applied electric field and at 1.32 μm, an electron/hole resonant effect is reported at ≈5 mW/cm^{-2}, in samples of zinc composition as high as 1%. This suggests a competition between electrons and holes. Table IX gives values of ξ_0 as a function of the wavelength, for samples of 4- and 1% zinc. One can conclude that the incorporation of zinc in the CdTe matrix has an important effect on the photorefractivity response of this material. The value of the electron-hole competition factor ξ_0 should thus lead to the choice of the appropriate stoichiometry of the crystal for the applications needed. In other words, for applications at 1.5 μm, it is obvious that crystals of zinc composition

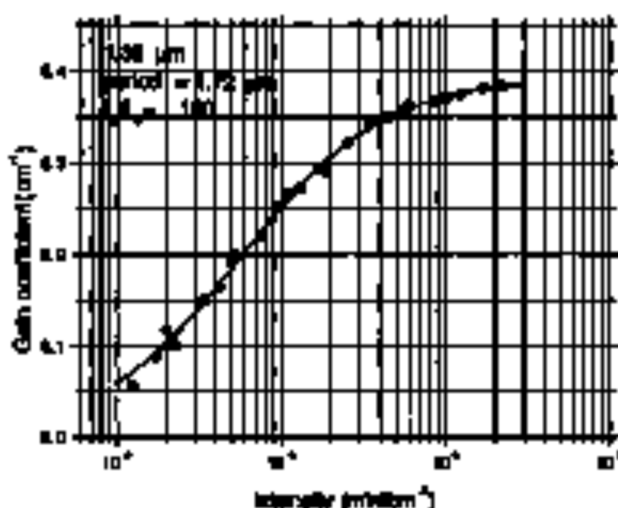

FIGURE 4.21 Two-beam coupling gain versus pump beam intensity at 300 K in CdZnTe (CZT), with 4% zinc [325]. The solid line is the theoretical fit to the gain given in Eq. (18). $\Gamma_{sat} = 0.398\ cm^{-1}$ and $I_d = 0.060\ mW/cm^2$, obtained from the curve fitting.

TABLE IX ξ_0 as a Function of the Wavelength for CZT Crystals of Two Different Zinc Compositions [410]

Zinc composition	0.04	0.01
Stoichiometry history	Stoichiometric	Tellurium rich
ξ_0 (1.048 μm)	−0.08	−0.65
Photoionized carrier	electron	electron
ξ_0 (1.32 μm)	+0.68	−0.35
Photoionized carrier	holes	electron
ξ_0 (1.550 μm)	+0.82	0.05
Photoionized carrier	holes	holes

of at least 4% are required (ξ_0 is positive and high). The other way, for applications at 1.048 μm, no incorporation of zinc in CdTe is necessary (ξ_0 is negative and high). Furthermore, it should be noted that Cd vacancies reduce the value of ξ_0.

Photorefractivity has been reported in bulk $Cd_{1-x}Mn_xTe$, for undoped crystals with zinc composition of 10% [327], and for semi-insulating vanadium-doped crystals with $x = 0.45$ (under applied electric field [112] and with no applied field [328]) and with $x = 0.33$ [329]. Photorefractive response was measured in the 0.6–1.0 μm range. The author in [327] demonstrates that at low temperatures, in a two-beam configuration, a magnetic field can control the direction and magnitude of photorefractive energy transfer by rotating the polarization of the beams inside the crystal. Morgan et al. [330] reported earlier photorefractivity in $CdS_{1-x}Se_x$ (vanadium doped), and a TBC gain of 0.20 cm^{-1} at 633 nm was measured [112].

More investigations need to be performed over a wider composition range, in order to determine more accurately the photosensitivity tunability ranges of these alloys.

3.2. Optical Limiters

There is an interest in using wide bandgap semiconductors as a basic material for IR power limiter (IRPL) applications. The feasibility of using doped CdTe crystals for photorefractive and, in particular for optical limiting applications, was examined by several authors [284,331–334].

The criteria for a successful semiconductor-based IRPL are:

(1) large electro-optic coefficient, r_{ij};
(2) high resistivity; and
(3) sufficiently high concentration of deep levels that can be photoionized to form free carriers and once ionized, become efficient trapping centers, which helps to maintain the space-charge field. Therefore, the depth of the level determines the long wavelength limit of the device.

The advantages of a semiconductor-based IRPL are:

(i) it is wavelength-agile;
(ii) it is self-actuating;
(iii) it has a wide-field-of-view (up to 10° full angle);
(iv) it has a very low power threshold (uses second order nonlinearity); and
(v) it limits both coherent and incoherent light.

For IRPL applications, the use of CdTe:V brings together a very desirable characteristics. The CdTe crystals have a direct gap of 1.5 eV, a wide transmission range (0.9–20 μ) with absorption coefficients as low as 0.0002 cm^{-1}, which when combined with their good thermomechanical properties offers the largest figure-of-merit for thermal fracture at 10.6 μ [335].

Cadmium telluride has already been shown to have a good figure-of-merit for device applications in the near IR:

a) it is a good photoconductor with a conductivity under illumination of $\sigma_{ph} \approx 2 \times 10^{-8}\ \Omega^{-1} cm^{-1}$, at 10 mW/cm^2;
b) it has a high dark resistivity, $\sigma_d \approx 2 \times 10^{-10}\ \Omega^{-1} cm^{-1}$, preventing the phenomenon of thermal runaway. Under these conditions, the device will not require cooling for heat dissipation. And
c) high figure-of-merit, $n_0^3 r_{41}$ = 130 pm/V; CdTe:V, for example, was shown to have a gain coefficient at 1.06 μ, more than twice as high as those of GaAs and InP [284].

Other nonlinearities in semiconductors, including two-photon absorption (TPA) and free carrier absorption, have also been studied and reviewed [340–343].

Both Si and GaAs were demonstrated as optical limiters based on nonlinear refraction effect [340,341]. Silicon has an indirect energy bandgap of 1.1 eV at room temperature. The Si optical limiter relies on linear indirect absorption ($\alpha \sim 10\ cm^{-1}$) of the 1.06 μm (1.17 eV) light to generate free carriers, which once generated are free to absorb additional photons (free carrier absorption). Gallium arsenide has a direct bandgap of 1.42 eV and thus the 1.06-μm radiation is insufficient for band-to-band excitation; however, TPA will occur for large

intensities. Optical limiters that rely on TPA phenomena have the potential to operate over a wider bandwidth than those that rely on single photon absorption. Similar studies have been performed on ZnSe for TPA-based optical limiting action, which has the potential of expanding broadband operation over the visible range [342].

3.3. Solid-State Midinfrared Tunable Lasers

Tunable mid-IR light sources are needed for a variety of applications such as optical communication systems, LIDAR, gas analyzers, and medical and scientific instrumentation, as well as target designation, obstacle avoidance, and IR countermeasures for the military.

Laser light sources continuously tunable in the near-IR spectral range, including the widely used Ti:sapphire [343], have been available for several years. This level of development has not been achieved in the 2–10-μm region, except for the $MgF_2:Co^{2+}$ laser [344], which has been tuned out to 2.5 μm. Today's available coherent sources include the cryogenic lead-salt diode lasers, gas and chemical lasers, a few rare-earth-ion lasers with limited tunability, and nonlinear optical devices such as Raman shifters and optical parametric oscillators (OPOs). In the mid-IR, the common explanation for the lack of strongly luminescent materials was the rapid onset of nonradiative decay associated with multiphonon recombination. Numerous reports dealt with the "undesired" IR luminescence generated by transition metal dopants (Cr, Co, Ni, and Fe) in visible light-emitting phosphors [345].

Solid-state lasers in the near- and mid-IR region, although not as widely tunable as the optical parametric oscillators/amplifier systems, have the advantage of compactness, especially when pumped by diode lasers. This opens the potential for transition metal-doped zinc chalcogenides (ZnS, ZnSe, and ZnTe doped with Cr^{2+}, Co^{2+}, Ni^{2+}, Fe^{+2}) for applications as room-temperature, mid-IR tunable laser media, as first demonstrated at Lawrence Livermore National Laboratory (LLNL) [55]. In particular, room-temperature laser demonstration of Cr^{2+}:ZnSe at 2.35 μm with a maximum slope efficiency of 20% has been achieved, with estimates of 75–100% quantum yields. The absorption, emission and nonradiative processes in Cr^{2+}-doped ZnSe, which are the basis for this four-level, solid-state laser, are shown in Figure 4.22. The small phonon frequencies of II-VI materials as compared to oxides and fluorides make nonradiative relaxation rates small at room temperature.

Tetrahedrally-coordinated Cr^{2+} ions are especially attractive as lasants as a result of their high luminescence quantum yields for emission in the 2–3 μm range. The ^5E radiative lifetimes and emission cross sections are, respectively,

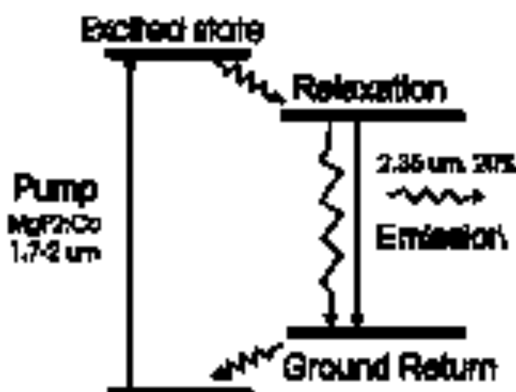

FIGURE 4.22 Absorption, emission and nonradiative processes in Cr^{2+}-doped ZnSe. The wavelength of 2.35 μm corresponds to the maximum intensity of emission in the tunability range.

~10 μs and ~10^{-18} cm^2 [63]. To date, the most impressive results have been obtained using the Cr^{2+} dopant. While the Co-doped crystals were shown to exhibit room-temperature quantum efficiencies that approach 100%, non-radiative decay appears to reduce Co and quench its luminescence [53]. The Cr^{2+} ion has been doped into several II-VI semiconductor materials. These materials include Zn and Cd chalcogenides [56,104]. Pulsed lasing has been demonstrated [346] with tunability extending from 2.13 to 2.8 μm and with slope efficiencies of >20%. The strong absorption features of the Cr-doped II–VI crystals match the output region of strained-layer InGaAs diode lasers and direct diode pumping of Cr^{2+}:ZnSe material has already been achieved [347]. A 2.6-μm, kHz repetition rate, Cr^{2+}:CdSe laser producing up to 815 mW was demonstrated at both the Air Force Research Lab and Cleveland Crystals [348]. Both Hampton University and Eclipse Corporation [349] are investigating the feasibility of the Cr^{2+}:CdMnTe system.

The first CW lasing in a transition metal doped II-VI compound was recently demonstrated by Coherent Technologies Inc., Fisk University, and LLNL with continuous tunability extending from 2.138 to 2.760 μm, output power of 250 mW with no active cooling, and slope efficiencies of 63% [350].

3.4. Optical Parametric Oscillators (OPO)

3.4.1. Principle

Another efficient way to obtain mid-IR radiation is to construct an optical parametric oscillator (OPO). Its principle of operation is based upon a process similar to harmonic generation, relying on the nonlinear response of a medium to a driving field (the pump laser beam) to convert a photon into two lower-energy photons.

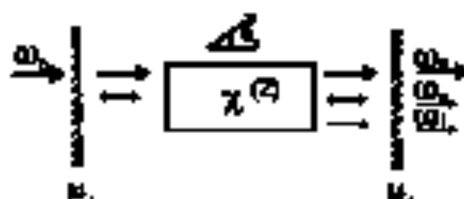

FIGURE 4.23 Basic configuration of an optical parametric oscillator.

(the signal and idler waves). Figure 4.23 shows the principle of operation of an optical parametric oscillator.

Energy conversion requires that the three photons be related by:

$$\omega_{pump} = \omega_{signal} + \omega_{idler} \tag{12}$$

while momentum conservation requires:

$$k_{pump} = k_{signal} + k_{idler} \tag{13}$$

The pair of frequencies satisfying Eq. (11) is not unique and, in general, Eqs. (11) and (12) cannot be satisfied simultaneously. The most efficient energy transfer occurs when all three waves travel at the same velocity, a "phase-matching" condition that can be met in birefringent crystals due to the variation of index of refraction with crystal orientation and wavelength. The wavelengths of the signal and idler will be determined by the θ_p angle defined as the one which the pump wavevector makes with the crystal axis; as the crystal rotates, different wavelengths of light are produced. Under phase-matched conditions, spontaneous emission of signal and idler occurs (amplification), with no exchange of energy with the medium.

To create an oscillator, the crystal is placed in a Fabry–Perot cavity that is resonant to the signal, the idler, or both, and a build-up of light output at the resonant wavelength will occur. The schematic of a singly resonant optical parametric oscillator is shown in Figure 4.23. In this case the dichroic cavity mirrors transmit at ω_p and reflect at ω_s.

For practical applications several factors need to be taken into account for selecting the optimal material: (i) large second-order nonlinear coefficient; (ii) large single crystals; (iii) adequate birefringence; (iv) high transparency; (v) large thermal conductivity and laser damage threshold; and (vi) good mechanical and chemical stability. The ideal NLO optical material for OPO applications should have a wide range of optical transmission and a small dependence of the refractive indices on temperature and high thermal conductivity. A recent review of the emergence of chalcopyrites as nonlinear optical materials was published [351].

3.4.2. Materials

The $LiNbO_3$ or KTP crystals pumped by a conventional Nd:YAG laser have been demonstrated to produce tunable IR radiation in the range of 1–5 μm. To extend the light source beyond the 5 μm range, bulk IR semiconductor materials have to be considered. We will review a few of the most promising materials for this type of application. Most of these materials have a chalcopyrite structure, as encountered in I-III-VI_2 and II-IV-V_2 classes of semiconductors. The chalcopyrite structure is similar to the zincblende one, with the group VI (or group V) element being tetrahedrally (slightly distorted) coordinated. The unit cell is tetragonal due to some uniaxial distortion of the lattice cell ($c/a \neq 2$, with 0–10% distortion), leading to interesting anisotropy (in particular, the birefringence is useful for devices) of the physical properties. A few examples of chalcopyrite semiconductors include $ZnGeP_2$, $CdGeAs_2$, $AgGaS_2$, $AgGaSe_2$ and others. Hexagonal (CdSe) and/or layer compound (GaSe) materials have the same useful property.

3.4.2.1. $ZnGeP_2$

Relative success was obtained in the $ZnGeP_2$ (ZGP) system; in spite of being intrinsically limited by 2- and 3-phonon absorptions of 0.3 cm^{-1}, it is currently considered one of the most promising materials. The transparency range of this material for stoichiometric, high-perfection crystals is from 0.62 to 13 μm; the relatively high thermal conductivity, the presence of adequate birefringence for phase matching, and the large nonlinear optical coefficient (d_{36} = 75 pm/V) make this material quite promising [352–354]. Absorption coefficients of 0.4–0.5 cm^{-1} at the CO_2-laser emission wavelengths limit the use of this crystal for frequency doubling but allow OPO applications in the 3–5 μm range. The temperature dependence of the birefringence and phase-matching conditions for $ZnGeP_2$ were studied [355].

The availability of high-quality crystals is somewhat limited by the complexity of the $ZnGeP_2$ system, involved are volatile and highly unstable reacting elements. Studies relating the growth condition, stoichiometry of as-grown and annealed crystals, point defects, and optical properties were published elucidating the nature of point-defect related optical absorptions [356,357]. A search for dopants for $ZnGeP_2$ aimed at reducing the concentration of native defects responsible for optical absorption bands that limit the OPO usability was also explored [358,359]. Calculations based on an atomistic description of the lattice predict that the group-III dopants will bind the hole more strongly than the group-I dopants [358].

Average output power as high as 10 W in the 3–5 μm region has been reported from a $ZnGeP_2$ OPO pumped at 2.05 μm by a pulsed Tm,Ho:YLF laser [360].

3.4.2.2 $CdGeAs_2$

Cadmium germanium arsenide ($CdGeAs_2$) is a chalcopyrite semiconductor known for having one of the highest nonlinear optical coefficients of any phase-matchable inorganic compound (d_{36} = 472 pm/V) [361], large birefringence $n_e - n_o \approx 0.1$ [362] sufficient for type-II phase matching, and a transparency range from 2.4 to 18 µm, making it attractive for CO_2-doubling, as well for as other mid-IR to FIR laser frequency conversion applications [264,363–365]. The typical as-grown material has a bandgap of 0.578 eV at 10 K, and a resistivity of 10 to 0.1 ohm-cm, corresponding to a free carrier concentration of 10^{16}–10^{17} cm^{-3} at room temperature [366]. More recently, crystals grown by the float zoning technique under microgravity have shown lower carrier concentrations in the lower 10^{15} cm^{-3} range [367].

The key elements in growing crack-free crystals are the use of low thermal gradients, seeded growth to avoid super-cooling and to control the orientation, and the use of a transparent furnace. In addition, feed purification and stoichiometry control can lower defect-related absorption losses below those of the best samples reported in the literature. An additional feature of $CdGeAs_2$ is its larger thermal conductivity (42–93 mW/cm·K) when compared with the I-III-VI_2 chalcopyrites, making it advantageous for both ease of crystal growth and a higher damage threshold, similar to that of Ge [368], for high-power laser applications. Current limitations include the RT intrinsic absorption by free carriers due to native defects, indicating a need for cryogenic operation. Up to 27% CO_2-doubling efficiencies and average output powers exceeding 1 W have been generated using $CdGeAs_2$ [369,370]. From more recent measurements [371], the nonlinear optical constant of $CdGeAs_2$, is $d_{36}(CdGeAs_2)$ = 4.7 times $d_{36}(AgGaSe_2)$ = 186 pm/V.

3.4.2.3 $AgGaS_2$, $AgGaSe_2$ and $AgGa_xIn_{1-x}Se_2$

Silver gallium sulfide and silver gallium selenide [372] combine large nonlinear coefficients (13.4 pm/V and 26.8 pm/V, respectively) with phase matching over a wide (0.5–12.5-µm) transmission range. Silver gallium sulfide is unique in its ability to be phase-matched when pumped at 1.06 µm. A review of the crystal growth and optical properties of this family of crystals was published [373] that included an evaluation of the mixed $AgGa_xIn_{1-x}Se_2$ previously proposed [374] for noncritical phase matching for CO_2 laser second harmonic generation. The effects of various dopants in $AgGaS_2$ and $AgGaSe_2$ were also described [359]. The best bulk absorption coefficient for $AgGaS_2$ at 1.06 µm was <0.0005 cm^{-1} [373], but surface absorption may increase with time.

Laser damage studies of $AgGaS_2$ by ESCA and Auger techniques have found that polished crystals have a silver-deficient layer ≈200 Å deep, while the bulk composition is close to stoichiometry [375]. The thermal conductivity for

$AgGaS_2$ and $AgGaSe_2$ at room temperature is 0.014 W/cm K and 0.011 W/cm K, respectively. This is significantly lower than the heat conductivity of $ZnGeP_2$, which is 0.35 W/cm K [375]. The growth of both $AgGaS_2$ and $AgGaSe_2$ is achieved by the Bridgman method using a c-axis oriented seed, which has a negative expansion coefficient, thus preventing the cracking of crystals during cooldown. The crystals have to be annealed in Ag_2S (or Ag_2Se) overpressure to eliminate the second-phase precipitation of Ga_2S_3 (Ga_2Se_3, respectively) causing light scattering [375]. Although this process restores the optical transmission of the crystals to almost theoretical values, they are not defect free, as they exhibit some degree of residual optical absorption and scattering.

A recent study [376] on the design and performance of an injection-seeded pulsed parametric oscillator OPO reports efficient difference frequency generation (DFG) in $AgGaSe_2$ and $AgGaS_2$ crystals. The maximum DFG conversion efficiency was obtained with a 2-cm-long $AgGaSe_2$ crystal, producing 3.6–16% quantum efficiency at ≈9.5 μm.

The mixed $AgGa_xIn_{1-x}Se_2$ crystals possess several advantages, including a maximum transparency coverage of the region of the CO_2-laser emission and its second harmonic, a high nonlinear quadratic susceptibility d_{36} compared with $AgGaSe_2$ and the possibility of achieving noncritical 90°-phase matching by selecting the value of $1 - x$ (indium content). This makes it possible to use longer crystals as well as prevents unwanted birefringence (drift) effects [377,378]. In a study reported in Reference [377], an efficiency of 10.5% for the Q-switched CO_2 laser radiation was achieved, which is superior to the performances of $AgGaSe_2$ and $ZnGeP_2$.

3.4.2.4. $AgGaTe_2$

A ternary chalcopyrite structural compound belonging to the I-III-VI_2 family, AGT has been the latest explored for NLO applications. The room-temperature bandgap is 1.32 eV and the melting point is 677°C [379]. Undoped, as-grown crystals are p-type. Although its nonlinear properties have not been reported, it belongs to a group of materials that have been very well studied, $AgGaS_2$ and $AgGaSe_2$. Ebel et al. [373] have investigated this crystal and reported good mechanical properties as well as the possibility of birefringence useful for nonlinear optics. They also estimate that the second-order nonlinear coefficient $\chi^{(2)}$ = 230 pm/V, and a figure-of-merit of 494 $(pm/V)^2$ is approximately 2.3 times that of $AgGaSe_2$.

The thermal conductivity of $AgGaTe_2$ was estimated [380] to be 0.9 W/m K by analysis of its bandgap trend within this semiconductor family. Based on the measured birefringence it was found [380] that this birefringence will not be sufficient for phase matching (Type I) at room temperature; however, accurate measurements of the indices of refraction are required before the conditions

for phase matching at elevated temperature are found. In the absorption spectrum, a band tail extending beyond the bandedge to 5–6 μm was observed in the as-grown crystals, indicating the presence of native defects. Chuner et al. proposed [380] the mixed $AgGa(Se_{1-x}Te_x)_2$ where x is chosen to provide the desired room temperature birefringence. It was estimated that a mixed crystal with $x = 19\%$ for a 10.6-μm pumped SHG process can exceed the conversion of $AgGaSe_2$ by >100%.

3.4.2.5. *CdSe*

Cadmium selenide is an attractive nonlinear crystal that can operate as an OPO in the 3.38–4.2 μm (signal) and the 8.3–12.6 μm (idler) regions. When pumped near 3 μm, CdSe has an effective nonlinear coefficient d_{eff} of 17–18 pm/V, and operates in a Type-II, phase-matched orientation with the angles ranging from 67 to 90° [381].

Reported absorption coefficients were nominally constant at 0.007–0.01 cm^{-1} over the 1–10 μm region. The thermal conductivity is moderately large, κ = 47 mW/cm-K. The birefringence and the indices of refraction of CdSe were measured in the 2.5–16.5 μm range [382]. The results of experiments in generating signal output centered at 3.9 μm by use of CdSe OPO have been reported [381]. More recently, a report on a CdSe OPO pumped by a 2.79 μm Cr, Er:YSGG laser oscillator yielding a 59% slope efficiency and 1.2–2.4 mJ of total idler output between 8.5 and 12.3 μm was published [383].

3.4.2.6. *GaSe*

Gallium selenide is a soft, layered material that can be cleaved only along the (001) plane, limiting the maximum length of the crystals to 1–2 cm. These crystals were successfully used for second harmonic generation of CO_2 laser radiation [348] and in type-II optical parametric generation in the 3.9–10 μm range [385]. The crystals have a high nonlinearity of 54.4 pm/V, which is approximately 10 times that of $LiNbO_3$. More recently, the largest wavelength range of tunability (3.3–19 μm) of an OPO was achieved in this material [386]. However, it was concluded that when a smaller tuning range (3.9–10 μm) is sufficient, $ZnGeP_2$ is superior because of its [illegible]-larger nonlinear figure-of-merit and availability of longer crystals, which makes the OPO pumping threshold one order of magnitude smaller and the quantum efficiency 2–3 times larger.

Gallium selenide has some interesting properties for nonlinear frequency conversion applications of IR laser light, either for second harmonic generation, also as difference frequency generation, or optical parametric oscillation, and an excellent review has been compiled by Fernelius [387]. It [illegible] in the

0.65–18-μm wavelength range, and the optical absorption coefficient remains below 1 cm^{-1} throughout the transparency range. Its nonlinear optical coefficient is also high. This material has been the subject of several studies [388–392] since the early 1970s, but difficulties in growing good material with the available techniques almost caused the efforts associated with GaSe to be abandoned.

Crystals of volatile or dissociable compounds, including many of the III–Vs and II–VIs, require a specialized growth technology. The growth problems stem from high vapor pressure and reactivity of the volatile component. Commercial gallium and selenium (6–9s pure) were further purified to remove residual impurities. The stoichiometric mixture was prepared by mixing elements Ga and Se. The temperature of the mixture was raised to 1050°C and maintained for many hours to ensure complete mixing. Crystal growth was carried out by the capillary-seeded Bridgman method. The details of the growth method are described in References [393,394]. It was carried out at a thermal gradient of 30°C/cm and the growth speed was 2 cm/day for growth of both doped and pure GaSe crystals. The X-ray powder diffraction pattern showed that the crystal belongs to hexagonal symmetry with $a = 0.375$ nm and $c = 1.595$ nm. The X-ray Laue patterns for the {001} plane were sharp and showed hexagonal symmetry. The details of the characterization of GaSe crystals can be found in Reference [395].

Due to crystal softness, bending and deformation is also very common among these crystals. The usual practice is to dope these crystals either with In or Ag, to improve their mechanical properties and fabricability. A detailed study on this issue and the characterization of the SHG and OPG fabricated from these crystals was reported [395].

In Reference [396], tunable mid-IR infrared down conversion with GaSe and $AgGaSe_2$ crystals over the 3.5–8.5 μm spectral range was achieved by difference frequency generation (DFG). Up to 10%-quantum conversion efficiency was demonstrated. The system also exhibits virtually no temporal delay between the pump and output pulses, which facilitates nonlinear optical interactions.

3.5. Infrared Optical Components

This section reviews some of the important infrared semiconductor materials used in the manufacture of windows, domes, substrates for infrared filters, and lenses. The main characteristics of these materials are their wide transmission range, low absorptivity, chemical stability, good mechanical strength, and stability for high-power applications, where thermal heating may occur. For example, windows for FIR lasers (such as CO_2) can undergo optical distortion of fraction of

high cw power levels due to their finite absorption coefficients [397,398]. The optical properties in the IR depend on the presence of native and foreign imperfections through absorption by free carriers, multiphonon processes, and on the presence of dislocations and precipitates through optical absorption or scattering [399]. Careful polishing and coating of the elements are essential processes for the fabrication of this type of optical components.

3.5.1. Zinc Selenide

Zinc selenide material is useful due to its full transmission in the 0.5–14 µm range and low dn/dT, making it particularly attractive for CO_2 laser applications [400]. Fracture toughness data (0.9 MPa·m$^{1/2}$) have been published for this material [401].

The ZnSe polycrystalline material is usually grown by chemical vapor deposition (CVD); it is chemically very stable and available in large sizes (up to 12-in diameter). It is the preferred material for lenses, windows, beam expanders, and output couplers.

3.5.2. Zinc Sulfide

The spectral range of 8–12 µm is a particularly useful one for the use of this material for applications such as front optics for harsh environments, forward looking infrared (FLIR) windows, and missile domes. For this spectral range, ZnS has higher transmittance (75% at 10.6 µm) [402] and durability than ZnSe. Fracture toughness data (1 MPa·m$^{1/2}$) have been published for this material [401]. The ZnS polycrystals are grown for these applications by CVD and specially postgrowth-treated crystals are also useful in the visible range of the spectrum.

3.5.3. *Germanium*

Germanium has a high refractive index ($n \sim 4$), which has a useful transmission range of 2–20 µm, low absorption coefficients (0.035 cm^{-1} at 10.6 µm), excellent mechanical properties, and availability in large sizes. One disadvantage is the high thermo-optic coefficient (dn/dT) of 40×10^{-5} K^{-1} at 10.6 µm.

Germanium is used to manufacture attenuated total reflection (ATR) prisms, beamsplitters, and optical filters for IR spectroscopy, as well as lens systems for thermal imaging. The low value of the bandgap (E_g = 0.66 eV) means that special precautions need to be taken to avoid the effect of thermal runaway. For materials in which free carrier absorption is significant, the absorption coefficient will increase with increasing temperature, which in turn will increase again the absorption coefficient until the material fractures. The thermal fracture

figure of merit for germanium is among the largest, surpassed only by that of GaAs [402].

3.5.4. Cadmium Telluride

Cadmium telluride has one of the widest IR transmission ranges: 1–25 μm. The absorptivity of single crystals of CdTe at 10.6 μm is <0.002 cm^{-1} [403]. In fact the calculated intrinsic absorption coefficient should be of the order of 10^{-8} cm^{-1} [404]. Its application for CO_2 lasers is limited to low CW power levels, due to its thermal conductivity. However, CdTe becomes the material of choice for filter substrates in the 12–25-μm region, where other materials possess low transmission due to the presence of multiphonon absorption bands.

A procedure for reducing the absorption coefficient at 10.6 μm (caused by precipitates) that involves the thermal annealing under a cadmium overpressure, was described [405]. The CdTe wafers were In doped with a concentration of 2×10^{17} indium atoms/cm^3 and thermal annealing took place in a region where $[V_{Cd}]$ is slightly greater than n, the concentration of electrons. In a similar study [406], the best conditions for preparation of CdTe with low absorption coefficient at 10.6 μm were 700°C at $p_{Cd} = 2 \times 10^{-3} - 3$ atm, for a 2-mm-thick sample doped with an indium concentration of 1.2×10^{17} cm^{-3}.

3.5.5. Gallium Arsenide

An alternative to zinc selenide is provided by gallium arsenide crystals, which are available in large quantities and sizes up to 10 cm because they are grown for optoelectronic devices. The refractive index of GaAs is $n \sim 3.3$ within the transparency range of 1.4–15 μm. Among its advantages is durability, especially when used in dusty environments. Unlike ZnSe, GaAs is attacked by most acids. The absorption coefficient is $\approx 10^{-2}$ cm^{-1} in high resistivity material. Impurities such as Cr and Fe absorb $\approx$3–5 μm range, which limits its use there [408]. The large bandgap gives a predicted critical power for thermal runaway of 20 kW at room temperature [407].

4. CONCLUSIONS

A variety of bulk semiconductors are being investigated for future needs, while some are already available and being used in IR technology for detection, modulation and generation of radiation. A particular interest exists in high-average-power devices operating the atmospheric windows of 3–5 μm (mid-IR) and 8–12 μm

TABLE X Room-temperature Bandgap and Refractive Index Values [361] for Elemental and Compounds Reviewed in this Chapter[a]

Material	Bandgap energy @ RT (eV)	Bandgap wavelength @ RT (μm)	Refractive index @ 10 μm
Ge	0.66	1.88	4.0
Si	1.1	1.06	3.4
InSb	0.17	7.3	4.2
InAs	0.36	3.5	3.8
GaSb	0.73	1.70	4.0
InP	1.35	0.92	3.5
GaAs	1.42	0.87	3.6
GaP	2.3	0.54	3.3
ZnTe	2.26	0.55	2.7
ZnSe	2.7	0.46	2.4
ZnS	3.65	0.34	2.4
CdTe	1.45	0.86	2.7
CdSe*	1.7	0.73	2.4
CdS*	2.3	0.54	2.3
GaSe*	2.0	0.62	2.8*
$AgGaTe_2$*	1.3	0.95	3.0* [380]
$AgGaSe_2$*	1.7	0.73	2.6*
$AgGaS_2$*	2.3	0.53	2.3*
$CdGeAs_2$*	0.57	2.2	3.6*
$ZnGeP_2$*	1.67	0.74	3.1*

[a]For convenience, the wavelength values corresponding to the bandgap energy were calculated. Materials marked with an asterisk exhibit birefringence.

(FIR) range, and tunable devices in these wavelength ranges are also highly desirable. Table X summarizes the main optical properties of the materials reviewed in this chapter. The main obstacle to more widespread use of such devices has been the difficulty in growing large, high-optical quality crystals, with a combination of high-nonlinear coefficients and optical and mechanical parameters compatible with those required for useful applications.

The information presented in this chapter should be considered as an overview and the reader should consider the references given here for a detailed understanding of each subject.

REFERENCES

1. [illegible]
2. [illegible]
3. [illegible]
4. [illegible]
5. [illegible]
6. [illegible]
7. [illegible]
8. [illegible]
9. [illegible]
10. [illegible]
11. [illegible]
12. [illegible]
13. [illegible]
14. [illegible]
15. [illegible]
16. [illegible]
17. [illegible]
18. [illegible]
19. [illegible]
20. [illegible]
21. [illegible]
22. [illegible]
23. [illegible]
24. [illegible]
25. [illegible]
26. [illegible]
27. [illegible]
28. [illegible]
29. [illegible]
30. [illegible]
31. [illegible]
32. [illegible]
33. [illegible]
34. [illegible]
35. [illegible]
36. [illegible]
37. [illegible]
38. [illegible]
39. [illegible]
40. [illegible]

41. A. [illegible], R. [illegible], R. [illegible], and D. [illegible], *J. Crystal Growth* 117, 10 (1992).
42. C. [illegible], R. Granger, [illegible], and R. Triboulet, *J. Crystal Growth* 79, 515 (1986).
43. C.-H. Su, S. L. Lehoczky, and F. R. Szofran, *J. Crystal Growth* 86, 87 (1988).
44. J. J. Kennedy, P. M. Amirtharaj, P. R. Boyd, S. B. Qadri, R. C. Dobbyn, and G. G. Long, *J. Crystal Growth* 86, 93 (1988).
45. Z. [illegible], J. [illegible], and J. [illegible], *J. Crystal Growth* 85, 227 (1988).
46. Y.-G. Sha, C.-H. Su, and S. L. Lehoczky, *J. Crystal Growth* 173, 88 (1997).
47. R. Triboulet, A. [illegible], B. [illegible], and R. Granger, *J. Crystal Growth* 79, [illegible] (1986).
48. R. Triboulet, *J. Crystal Growth* 86, 79 (1988).
49. J.-O. Ndap, [illegible], Université de Paris [illegible], [illegible].
50. H. L. Glass, A. J. Socha, C. L. Parfeniuk, and D. W. Bakken, *J. Crystal Growth* 184/185, 1035–1038 (1998).
51. H. L. Glass, A. J. Socha, D. W. Bakken, V. M. [illegible], and J. P. Flint, *Mat. Res. Soc. Proc.* 487, 27–32 (1998).
52. J. Zhu, X. Huang, B. Li, and J. Chu, *Infrared Physics & Technology* 40, 411 (1999).
53. H. H. [illegible], T. O. Henderson, A. Burger, and M. F. [illegible], *Appl. Phys. Lett.* [illegible] (1999).
54. W. F. Krupke, R. H. Page, L. D. DeLoach, and S. A. Payne, U.S. Patent [illegible], 1996.
55. L. D. DeLoach, R. H. Page, G. D. Wilke, S. A. Payne, and W. F. Krupke, *IEEE J. Quantum Electron.* 32, 885 (1996).
56. B. [illegible], X. [illegible], Y. R. [illegible], R. R. [illegible], E. [illegible], R. J. [illegible], and R. W. [illegible], *Opt. Lett.* 22, 1180 (1997).
57. B. [illegible], M. [illegible], A. [illegible], J. T. [illegible], H. [illegible], R. R. [illegible], R. W. [illegible], C. C. [illegible], R. J. [illegible], P. R. Boyd, and W. [illegible], "Mid-Infrared Luminescence Properties of Cr^{2+} and Co^{2+} Doped CdSe and CdMnTe," Presented at the CLEO annual meeting, Baltimore, May 1999.
58. A. I. [illegible], N. I. [illegible], V. A. [illegible], A. L. [illegible], Y. B. [illegible], and A. I. [illegible], *Sov. Phys. JETP* 67 (4), [illegible] (1988).
59. M. [illegible], M. Godlewski, and T. P. Surkova, *Phys. Rev. B* 58, [illegible] (1998).
60. V. Yu. Ivanov, Yu. G. Semenov, M. Surma, and M. Godlewski, [illegible] 54, 4696 (1996).
61. T. [illegible], H.-T. Chen, B. Chen, and A. Burger, "Chromium Diffusion Doping on ZnSe Crystals" ACCG-east, Atlantic City, NJ, 1999.
62. A. Burger, J.-O. Ndap, K. Chattopadhyay, X. Ma, and R. B. [illegible], to be published.
63. R. H. Page, L. D. DeLoach, K. I. Schaffers, F. D. Patel, R. J. Beach, S. A. Payne, W. F. Krupke, and A. Burger, "OSA TOPS on Advanced Solid-State Lasers," Vol. 1, pp. 130–136 (Stephen A. Payne and Clifford Pollock, Eds.), Optical Society of America, Washington, DC, 1997.
64. K. [illegible], Transition Metal Doping of ZnSe, Summer Program for Undergraduates, Research Report, Fisk University, Nashville, TN, 1998.
65. I. [illegible] and M. [illegible], *J. Crystal Growth* 41, 103 (1977).
66. A. [illegible], K. [illegible], and T. [illegible], *Japan J. Appl. Phys.* 10, 1963 (1971).
67. I. [illegible] and M. [illegible], *J. Crystal Growth* 46, 457 (1979).
68. M. P. Kulakov, I. B. [illegible], and A. V. Fadeev, *J. Crystal Growth* 52, 609 (1981).
69. P. Rudolph, P. [illegible], and N. [illegible], *Materials Science and Engineering Reports* 15, 85 (1995).
70. R. [illegible], [illegible] *Sci.* [illegible] 8, [illegible] (1958).
71. B. J. Fitzpatrick, T. F. McGee, and P. M. Harnack, *J. Crystal Growth* 78, 242 (1986).
72. H. [illegible], T. [illegible], A. [illegible], and Y. [illegible], *J. Crystal Growth* 117, 75 (1992).
73. R. Triboulet, F. [illegible], R. Legros, H. Lozykowski, and G. Didier, *J. Crystal Growth* 59, 172 (1982).
74. T. [illegible], H. [illegible], and M. [illegible], *J. Crystal Growth* 171, 39 (1997).

75. Y. [illegible], H. [illegible], Y. [illegible], and S. [illegible], *Materials Transactions JIM* [illegible] (1995).
76. S. [illegible] and H. [illegible], *J. Crystal Growth* [illegible] (1995).
77. S. Fujiwara, H. [illegible], T. [illegible], K. Matsumoto, and T. [illegible], *J. Crystal Growth* [illegible] (1996).
78. J. [illegible] and [illegible], *Mat. Letters* [illegible] (1995).
79. S. [illegible], *J. Crystal Growth* [illegible] (1995).
80. [illegible], *J. Crystal Growth* [illegible] (1995).
81. [illegible] and [illegible], *J. Crystal Growth* [illegible] (1996).
82. [illegible] and [illegible], *J. Crystal Growth* [illegible] (1997).
83. G. [illegible], [illegible], and [illegible], *J. Appl. Phys.* [illegible] (1998).
84. S. [illegible], *J. Crystal Growth* [illegible] (1994).
85. K.-T. Chen, M. A. George, Y. [illegible], A. Burger, C.-H. Su, Y.-G. Sha, D. C. Gillies, and S. L. Lehoczky, *J. Crystal Growth* [illegible] (1995).
86. C.-H. Su, Y.-G. Sha, [illegible], S. L. Lehoczky, [illegible], and R. F. [illegible], *J. Crystal Growth* [illegible] (1996).
87. Y. V. Korostelin, [illegible], and [illegible], *J. Crystal Growth* [illegible] (1996).
88. [illegible], *J. Crystal Growth* [illegible] (1996).
89. A. [illegible], L. [illegible], and [illegible], *J. Crystal Growth* [illegible] (1998).
90. S. [illegible], *Jap. J. Appl. Phys.* [illegible] (1996).
91. [illegible], *Phys. Stat. Sol.* [illegible] (1996).
92. S. Fujiwara, [illegible], and [illegible], *J. Crystal Growth* [illegible] (1996).
93. T. [illegible], *Appl. Sur. Sci.* [illegible] (1996).
94. E. Tournié, J.-O. Ndap, A. [illegible], A. T. [illegible], and [illegible], *Journal de Physique* [illegible] (1995).
95. E. Tournié, J.-O. Ndap, A. T. [illegible], and [illegible], *J. Crystal Growth* [illegible] (1996).
96. [illegible], *J. Phys. Solid State Phys.* [illegible] (1976).
97. A. [illegible], M. J. [illegible], and A. Burger, *Phys. Rev.* [illegible] (1988).
98. C. I. Rablau, J.-O. Ndap, [illegible], A. Burger, and N. C. Giles, *J. Electron. Mater.* [illegible] (1999).
99. R. H. Page, [illegible], and A. Burger, *IEEE J. Quantum Electron.* [illegible] (1997).
100. Eagle-Picher Industries, Inc., [illegible] (1994).
101. Y. K. Du, [illegible], *Chem. Mater.* [illegible] (1992).
102. [illegible], *J. Crystal Growth* [illegible] (1993).
103. [illegible], *J. Crystal Growth* [illegible] (1995).
104. [illegible], *J. Luminescence* [illegible] (1997).
105. B. C. [illegible], *Phys. Rev.* [illegible] (1995).
106. J.-O. Ndap, [illegible], C. I. Rablau, [illegible], and A. Burger, Discussion Paper, ACCGE-11, August [illegible], [illegible] (to be published) in *J. Crystal Growth*.
107. [illegible], *Japan J. Appl. Phys.* [illegible] (1975).
108. A. Burger, [illegible], *IEEE Trans. Nucl. Sci.* [illegible].
109. A. Burger and M. Roth, *J. Crystal Growth* [illegible].
110. E. Tournié and [illegible], *J. Crystal Growth* [illegible].
111. S. W. [illegible], [illegible], and J. T. [illegible], Discussion Paper, ACCGE/East—September [illegible], Atlantic City, NJ [illegible].

112. G. A. [illegible], K. M. [illegible], and K. E. [illegible], *Opt. Mater.* 4, 234 (1995).
113. A. Burger, K. Chattopadhyay, H. Chen, J.-O. Ndap, X. Ma, S. E. Trivedi, S. W. Kutcher, R. Chen, and R. D. Rosemeier, *J. Crystal Growth* 198/199, 872 (1999).
114. A. Y. Wu and R. J. Sladek, *J. Appl. Phys.* 53, 8589 (1982).
115. [illegible] Corp. of America, [illegible] Blvd. Baltimore, MD, 21236-4968 (US).
116. K. [illegible], A. [illegible], and J. [illegible], *J. Crystal Growth* 104, 131 (1990).
117. M. [illegible], A. [illegible], R. [illegible], E. [illegible], and H. [illegible], *J. Crystal Growth* 128, 588 (1993).
118. W. H. [illegible] and M. [illegible], *Appl. Phys. Lett.* 53, [illegible] (1988).
119. T. Y. [illegible], [illegible], J. H. [illegible], and M. [illegible], *Mat. Res. Soc. Symp. Proc.* [illegible], [illegible] (1995).
120. P. [illegible] and K. [illegible], *J. Crystal Growth* 48, 24, (1980).
121. K. [illegible], *J. Crystal Growth* 51, 453 (1981).
122. H. [illegible] and C. H. [illegible], *J. [illegible]* 22, 1120, (1995).
123. C. [illegible], M. [illegible], and R. [illegible], *J. Crystal Growth* 83, 306 (1988).
124. K. [illegible], U. [illegible], A. [illegible], R. R. [illegible], J. [illegible], A. [illegible], and E. [illegible], *J. Crystal Growth* 123, 510 (1992).
125. Y. [illegible], M. [illegible], K. [illegible], E. [illegible], and Y. [illegible], *J. Crystal Growth* 1[illegible], 3[illegible] (1992).
126. E. [illegible], Y. [illegible], Y. [illegible], T. [illegible], T. [illegible], and M. [illegible], *J. Crystal Growth* 13[illegible], [illegible] (1997).
127. C. [illegible], G. [illegible], D. [illegible], and D. [illegible], *J. Crystal Growth* 21, 227 (1974).
128. K. [illegible] and H. J. [illegible], *J. Crystal Growth* 48, 471 (1980).
129. C. J. Johnson, *Proc. SPIE* 1106, 56 (1989).
130. A. [illegible], A. [illegible], and M. [illegible], *J. Appl. Phys.* 64, 3459 (1988).
131. A. [illegible], Y. [illegible], and W. [illegible], *J. Crystal Growth* [illegible], 127 (1988).
132. M. [illegible], H.-J. [illegible], R. [illegible], and U. [illegible], *J. Crystal Growth* 104, 295 (1990).
133. M. [illegible], P. [illegible], C. [illegible], R. [illegible], and G. [illegible], *J. Crystal Growth* 101, 2[illegible] (1990).
134. Y.-C. [illegible], J. J. [illegible], and R. A. [illegible], *J. Crystal Growth* 102, 807 (1990).
135. M. [illegible], P. [illegible], and A. [illegible], "Proc. 3rd European Conf. On Crystal Growth" (ECCG-3), [illegible], 1991.
136. R. S. [illegible], S. [illegible], S. [illegible], and D. J. [illegible], *J. Vacuum Sci. Technol.* [illegible], 1[illegible] (1991).
137. P. [illegible], M. [illegible], and M. [illegible], *J. Crystal Growth* 128, 582 (1993).
138. P. [illegible], *Prog. Crystal Growth and Charact.* 29, 275 (1994).
139. A. [illegible], [illegible] CdTe [illegible] [illegible], Ph.D. Dissertation (Université de Paris XI Orsay-[illegible], 199[illegible]).
140. K. Zanio, in "Semiconductors and Semimetals," Vol. 13, Academic Press, New York, 1978.
141. K. Y. [illegible], D. [illegible], A. [illegible], R. E. [illegible], and C. J. Johnson, *J. Crystal Growth* 86, 118 (1988).
142. P. [illegible], D. [illegible], D. [illegible], and R. Triboulet, *J. Crystal Growth* 101, 270 (1990).
143. P. [illegible], A. [illegible], D. [illegible], A. [illegible], and R. Triboulet, *Mat. Sci. Engineering* B16, 84 (1993).
144. E. [illegible] and J. F. [illegible], *IEEE Trans. Nucl. Sci.* 35, 84 (1988).
145. A. [illegible], Y. [illegible], B. [illegible], and T. [illegible], *Mater. Res. Soc. Symp. Proc.* 90, 111 (1987).
146. M. [illegible], A. [illegible], D. [illegible], and M. [illegible], *J. Crystal Growth* 101, 258 (1990).
147. R. Triboulet, Y. [illegible], A. [illegible], and P. [illegible], *J. Appl. Phys.* 45, 2759 (1974).
148. R. [illegible], R. [illegible], and R. [illegible], *J. Crystal Growth* 72, 22 (1985).

149. R. Triboulet, [illegible], and D. [illegible], *J. Crystal Growth* 72, [illegible] ([illegible]).
150. R. Triboulet, [illegible], and G. Didier, *J. Crystal Growth* 101, [illegible] ([illegible]).
151. [illegible], R. Triboulet, A. [illegible], [illegible], and G. Didier, *J. Crystal Growth* [illegible], [illegible] (199[illegible]).
152. H.-Y. [illegible] and C.-Y. [illegible], *J. Crystal Growth* [illegible], 67 ([illegible]).
153. [illegible], J. A. [illegible], C. V. [illegible], and J. [illegible], *J. Electron. Mat.* 4, [illegible] ([illegible]).
154. [illegible], and R. [illegible], *Mat. Science Forum* [illegible] ([illegible]).
155. M. A. [illegible], and [illegible], [illegible] *Mat.* [illegible] ([illegible]).
156. P. Rudolph, [illegible], and [illegible], [illegible] ([illegible]).
157. [illegible], and J. [illegible], *Mat. Res. Soc. Symp. Proc.* [illegible] ([illegible]).
158. [illegible], M. [illegible], and J. [illegible], *Nuclear Instruments and Methods in Physics Research* A[illegible], [illegible] ([illegible]).
159. [illegible] and [illegible], *J. Crystal Growth* [illegible], [illegible] ([illegible]).
160. H.-Y. [illegible] and C.-Y. [illegible], *J. Crystal Growth* 1[illegible], [illegible] (199[illegible]).
161. [illegible], *Solid State Comm.* [illegible] ([illegible]).
162. [illegible], and [illegible], in "Digest of Topical Meeting on [illegible] Materials, [illegible] and Devices", The Optical Society of America, Washington, DC, V. 14, p. [illegible], 199[illegible].
163. [illegible], and [illegible], *J. Crystal Growth* [illegible], [illegible] ([illegible]).
164. [illegible], and [illegible], *J. Crystal Growth* [illegible], [illegible] ([illegible]).
165. [illegible], and [illegible], *J. Crystal Growth* [illegible], [illegible] ([illegible]).
166. [illegible] and [illegible], *J. Crystal Growth* [illegible], [illegible] ([illegible]).
167. A. [illegible] and [illegible], *Phys. Rev.* [illegible], [illegible] ([illegible]); [illegible], [illegible] ([illegible]).
168. [illegible], and [illegible], *Cryst. Res. Technol.* [illegible], [illegible] (199[illegible]).
169. [illegible], and [illegible], *Nuclear Instruments & Methods in Physics Research, Section A—Accelerators Spectrometers Detectors and Associated Equipment* [illegible], [illegible] ([illegible]).
170. [illegible], and C. L. [illegible], *Nuclear Instruments & Methods in Physics Research, Section A—Accelerators Spectrometers Detectors and Associated Equipment* [illegible], [illegible] (199[illegible]).
171. [illegible], and C. L. [illegible], *IEEE Trans. Nuclear Science* [illegible], [illegible] (199[illegible]).
172. [illegible], [illegible] ([illegible]).
173. [illegible], *Pure and Appl. Phys.* [illegible], [illegible] ([illegible]).
174. [illegible], and [illegible], *Solar Energy Materials and Solar Cells* [illegible], [illegible] (199[illegible]).
175. [illegible], *J. Electron. Mat.* [illegible], [illegible] ([illegible]).
176. [illegible], *Nuclear Instruments & Methods in Physics Research, Section A—Accelerators Spectrometers Detectors and Associated Equipment* [illegible], [illegible] (199[illegible]).

177. J. W. Chen, T. [illegible], J. [illegible], M. [illegible], T. [illegible], M. [illegible], K. [illegible], D. G. [illegible], M. [illegible], and P. [illegible], *Nuclear Instruments & Methods in Physics Research, Section A: Accelerators, Spectrometers, Detectors and Associated Equipment* 365, 273 (1995).
178. P. J. Sellin, C. M. Buttar, S. Manolopoulos, K. [illegible], M. R. [illegible] and M. Cowperthwaite, *IEEE Trans. Nuclear Science* 42, 247 (1995).
179. M. B. Klein, *Opt. Lett.* 9, 350 (1984).
180. A. M. Glass, A. M. Johnson, D. H. Olson, W. Simpson, and A. A. Ballman, *Appl. Phys. Lett.* 44, 948 (1984).
181. H. Wenzl, "MRS Spring Meeting, SYMPOSIUM T, *Advanced Semiconductor Wafer Engineering*," April 5–7, 1999.
182. M. [illegible], K. W. [illegible], and H. Wenzl, *J. Crystal Growth* 175, 426 (1997).
183. W. A. Oates, O. Eriksson, and H. Wenzl, *J. Alloys and Compounds* 220, 48 (1995).
184. M. R. Brozel and G. E. Stillman (Eds.), "Properties of Gallium Arsenide", 3rd edition INSPEC, IEE Books, London, UK, 1996.
185. A. [illegible], A. [illegible], and H. [illegible], *J. Appl. Phys.* 47, 3025 (1976).
186. D. B. Thompson, J. D. McMullen, and D. B. Anderson, *Appl. Phys. Lett.* 29, 113 (1976).
187. L. A. Gordon, G. L. Woods, R. C. Eckardt, R. K. Route, R. S. Feigelson, M. M. Fejer, and R. Byer, *Electron. Lett.* 29, 1942 (1993).
188. L. A. Gordon, J. L. [illegible], Y. K. [illegible], R. C. Eckardt, R. K. Route, R. S. Feigelson, M. M. Fejer, and R. L. Byer, invited paper CLEO Pacific Rim, July 1995.
189. Y. [illegible], R. S. Feigelson, R. K. Route, D. Zheng, L. A. Gordon, M. M. Fejer, and R. L. Byer, *Mat. Res. Soc. Symp. Proc.* 484, 483 (1998).
190. L. B. [illegible], "The [illegible] of Growing Crystals", Chapter 19, pp. 381–397 (J. J. Gilman, Ed.), John Wiley & Sons, New York, 1963.
191. S. H. Liu and S. Kou, *J. Crystal Growth* 152, 230 (1995).
192. G. N. Kozhemyakin, *J. Crystal Growth* 149, 266 (1995).
193. T. [illegible], Y. [illegible], Y. [illegible], and M. [illegible], *J. Electron. Mater.* 19, 148[illegible] (1990).
194. D. C. Miller and A. F. Witt, *J. Crystal Growth* 29, 19 (1975).
195. D. C. Miller, *J. Crystal Growth* [illegible], 31 (197[illegible]).
196. S. W. [illegible] and G. Müller, *J. Crystal Growth* 46, 33 (1979).
197. P. B. Yip and W. R. Wilcox, *J. Crystal Growth* 36, 28 (1976).
198. J. Zhou, M. Larrousse, W. R. Wilcox, and L. L. Regel, *J. Crystal Growth* 128, 173 (1993).
199. T. A. Campbell and Jean N. Koster, *J. Crystal Growth* 178, 258 (1997).
200. T. A. Campbell and Jean N. Koster, *J. Crystal Growth* 171, 1 (1997).
201. M. N. [illegible], A. V. [illegible], A. R. [illegible], N. V. [illegible], A. S. [illegible], and B. B. [illegible], [illegible] 27, [illegible] (1981).
202. M. [illegible], K. [illegible], R. [illegible], and N. [illegible], *J. Crystal Growth* 176, 245 (1997).
203. C. E. T. White and H. Okamoto, "Phase Diagrams of Indium Alloys and their Engineering Applications (1)," p. 254, ASM International, USA, 1992.
204. S. R. [illegible], V. H. [illegible], and T. H. Myers, *Mat. Res. Soc. Symp. Proc.* 90, 429 (1987).
205. R. A. [illegible], [illegible] *Sci. Technol.* 6, C53 (1991).
206. "[illegible] Infrared Detectors, Theory and Application," company literature, Fairfield, CT, 1998.
207. EG&G Optoelectronics — Judson, *Infrared Detectors*, company literature, Montgomeryville, PA, 1998.
208. P. [illegible], R. [illegible], S. [illegible] Babu, P. Santhanaraghavan, and P. Ramasamy, *J. Crystal Growth* 204, 95 (1999).
209. J. [illegible] and K. Suto, *J. Appl. Phys.* 51, 2429 (1980).
210. K. [illegible] et al., *J. Appl. Phys.* 21, 797 (1982).
211. T. Miya, Y. Terunuma, T. Hosaka, and T. Miyashita, *Elect. Lett.* 15, 106 (1979).
212. D. N. Payne and W. A. Gambling, *Elec. Lett.* 11, 176 (1975).

213. L. G. Cohen and C. Lin, *Appl. Optics* 16, 3136 (1977).
214. H. Asahi, [illegible] 38 (1984).
215. S. [illegible], K. [illegible], M. [illegible], M. [illegible], T. [illegible], and A. [illegible], "[illegible] Proceedings of the Semiconductor [illegible] Seminar" (in Japanese), p. [illegible] (1985).
216. Y. [illegible], K. [illegible], and K. [illegible], *Semiconductor World* [illegible] 1985).
217. Y. [illegible], A. [illegible], and J. [illegible], *Hitachi* [illegible] (in Japanese), [illegible] (1985).
218. A. S. [illegible], *J. Crystal Growth* 71, 539 (1985).
219. M. [illegible] and M. [illegible], *Semiconductor World* [illegible] July 1985).
220. J. A. [illegible], *J. Crystal Growth* 60, 141 (1982).
221. J. A. [illegible], *J. Crystal Growth* 64, 1 (1983).
222. [illegible], K. [illegible], E. [illegible], O. Oda, and H. Asahi, "Extended Abstracts," p. 743, The Jpn. Soc. Appl. Phys., 1985.
223. K. [illegible], Y. [illegible], M. [illegible], and T. [illegible], "Extended Abstracts," p. 195, The Jpn. Soc. Appl. Phys., 1987.
224. W. A. [illegible], *J. Crystal Growth* 54, 21 (1981).
225. J. E. [illegible], G. J. [illegible], E. A. [illegible], D. A. E. [illegible], J. K. [illegible], and A. J. Thompson, *J. Crystal Growth* 64, 15 (1983).
226. M. [illegible], H. [illegible], and H. Asahi, "Extended Abstracts," p. 630, The Jpn. Soc. Appl. Phys., 1987.
227. T. [illegible], T. [illegible], M. [illegible], and T. [illegible], *Appl. Phys. Lett.* 50, [illegible] (1987).
228. S. K. [illegible] and G. A. [illegible], NATO Sponsored InP Workshop, 1986, p. 1[illegible].
229. K. [illegible] and J. [illegible], *J. Crystal Growth* 68, [illegible] (1984).
230. J. M. [illegible] Jr. and F. A. [illegible], *J. Crystal Growth* 73, 211 (1985).
231. H. M. [illegible], H. A. [illegible], F. [illegible], and P. [illegible], *J. Crystal Growth* [illegible], [illegible] (1977).
232. O. M. [illegible] and W. K. [illegible], *Acta [illegible]* 16, 315 (1977).
233. K. J. [illegible], E. [illegible], J. L. [illegible], and K. A. [illegible], *J. [illegible]* 4, 349 (1975).
234. W. A. [illegible], *J. Crystal Growth* 54, 21 (1981).
235. J. J. [illegible] and K. A. [illegible], *J. Crystal Growth* 74, [illegible] (1986).
236. J. J. [illegible] and K. A. [illegible], *J. Crystal Growth* 74, 277 (1986).
237. S. [illegible], S. [illegible], and C. [illegible], "Proc. of the Ninth Int. Conf. on GaAs and Related Compounds," [illegible], Japan.
238. O. [illegible], J. [illegible], and M. [illegible], *J. Crystal Growth* 65, 90 (1983).
239. E. [illegible], S. [illegible], A. [illegible], O. Oda, H. Asahi, and I. [illegible], "Proc. of the 12th Int. Symposium on GaAs and Related Compounds," [illegible], Japan, 1985, p. 67.
240. S. [illegible], Ph.D. Dissertation, [illegible] University, 1985.
241. S. [illegible] and C. [illegible], [illegible] (in Japanese) 21, 335 (1985).
242. A. [illegible], S. [illegible], M. [illegible], E. [illegible], and S. [illegible], "Proc. of the 4th Int. Conf. on Semi-Insulating III-V Materials," [illegible], Japan, 1986, p. 41.
243. G. W. [illegible] and K. S. [illegible], *Appl. Phys. Lett.* 48, 1026 (1986).
244. C. D. [illegible], A. H. [illegible], L. M. [illegible], Y. T. [illegible], T. [illegible], J. [illegible], and H. C. [illegible], *Appl. Phys. Lett.* 48, 1160 (1986).
245. C. E. [illegible], G. A. [illegible], and C. [illegible], *J. Crystal Growth* 54, 2[illegible] (1983).
246. H. [illegible] and K. [illegible], *J. Appl. Phys.* 52, 2[illegible] (1981).
247. B. [illegible], G. T. [illegible], W. R. [illegible], and W. H. K. [illegible], *J. [illegible]* 16, 3[illegible] (198[illegible]).
248. G. [illegible], R. M. [illegible], and M. [illegible], "Semi-Insulating III-V Materials", "Proc. of the Conf. on Semi-Insulating III-V Materials," Nottingham, UK, 1980, p. 3[illegible].
249. I. R. [illegible], M. A. [illegible], E. [illegible], and W. R. [illegible], *J. Crystal Growth* 64, 115 (1983).
250. K. [illegible], H. [illegible], H. [illegible], T. [illegible], and O. Oda, "Proc. of the 16th Int. Symposium on GaAs and Related Compounds," [illegible], Japan, 1989.

251. R. K. Willardson and Albert C. Beer, (Eds.), "Semiconductors and Semimetals" 13, Academic Press, New York, 1983.
252. A. Sawada, M. [illegible], and Y. Takeda, Jpn. J. Appl. Phys. 19, [illegible] ([illegible]).
253. T. H. Chen, J. L. Zyskind, and W. T. Tsang, J. Electron. Mater. 16, 57 (1987).
254. M. J. Cheung, G. B. Stringfellow, D. W. Kisker, A. K. Srivastava and J. L. Zyskind, Appl. Phys. Lett. 48, 495 (1986).
255. R. C. Gross, in "Materials Processing in the Reduced Gravity Environment of Space," p. 355 (G. Rindone, Ed.), North Holland, Amsterdam, 1982.
256. C. R. Lopez, J. R. Williams, and R. Abbaschian, J. Crystal Growth 200, 1 (1999).
257. "The Second NREL Conference on Thermophotovoltaic Generation of Electricity" (J. Benner, T. Coutts, and D. Ginley, Eds.), Am. Inst. Phys. Proc. 358, Woodbury, NY, 1996.
258. J. R. Boyer and W. T. Nelson, Mat. Res. Soc. Symp. Proc. 483, 46 (1998).
259. P. G. Schunemann and T. M. Pollak, U.S. Patent 5,611,856, 1997.
260. P. G. Schunemann and T. M. Pollak, J. Crystal Growth "Proceedings of the 1996 10th American Conference on Crystal Growth and the 9th International Conference on Vapor Growth and Epitaxy," Aug. 4–9 1996, 174, 1–4 Apr. 2 1997, Vail CO, pp. 272–277, 1993.
261. A. S. Borshchevsky, N. K. [illegible], and R. B. [illegible], Mater. Res. Bull. 19, 409 (1980).
262. M. [illegible] and F. [illegible], J. Mat. Sci. Lett. 13, 1229 (1994).
263. M. Zied Saghir and V. [illegible], in "Heat Transfer in Microgravity Systems Proceedings of the 1996 International Mechanical Engineering Congress and Exposition," Nov. 6–11, 1994, Vol. 290, p. 9, 1995.
264. M. Z. Saghir, D. Labrie, A. Ginovker, B. E. Paton, A. E. George, K. [illegible], and A. M. Simpson, J. Crystal Growth 256, 190 (2003).
265. R. P. [illegible], M. [illegible], and B. [illegible], J. Electronic Materials 19, 777 (1990).
266. G. C. Xing, K. J. Bachmann, and J. B. Posthill, Appl. Phys. Lett. 56, 271 (1990).
267. R. A. Mingled, A. J. Payne, and B. Kipp, J. Mat. Res. 4, 693 (1990).
268. E. M. Gallegos, T. Henningsen, R. M. Thomas, and R. H. Hopkins, Westinghouse Science and Technology Center Final Report WL-TR-94-4063, 1995.
269. A. W. Vere, L. L. Taylor, B. C. Smith, C. J. Flynn, M. K. Saker, and J. Jones, Mat. Res. Soc. Symp. Proc. 354, 495 (1995).
270. N. C. Giles and L. E. Halliburton, MRS Bulletin 23, 37 (1998).
271. B. R. [illegible], V. Yu. Rud', and Yu. V. Rud', Mat. Res. Bull. 23, 41 (1988).
272. Yu. M. Andreev, I. S. Baturin, P. P. Geiko, and A. I. Gusamov, Quantum Electronics 29, 403 (1999).
273. B. Tell, L. J. Frey, and H. M. Kasper, Phys. Rev. B 9, 5203 (1974).
274. P. G. Schunemann and T. M. Pollak, Lockheed Sanders Final report WL-TR-93-4XXX, 1993.
275. Yu. V. Rud and R. V. Masagutova, Sov. Tech. Phys. Lett. 7, 72 (1981).
276. V. N. Brudnyi, D. L. Budnitskii, M. A. Krivov, R. V. Masagutova, V. D. Prochukhan, and Yu. V. Rud, Phys. Stat. Sol. A50, 379 (1978).
277. P. G. Schunemann, S. J. [illegible], M. G. [illegible], W. C. Mitchel, and R. C. Fernelius, Mat. Res. Soc. Symp. Proc. 396, 729 (1995).
278. I. Zwieback, [illegible] Inc., final report [illegible], 1993.
279. P. G. Schunemann, P. J. Drevinsky, and M. C. Ohmer, Mat. Res. Soc. Symp. Proc. 354, 379 (1995).
280. G. D. Watkins in "Radiation Damage in Semiconductors," p. 97 (P. Baruch, Ed.), Dunod, Paris, 1965.
281. M. H. Rakowsky, W. K. Kuhn, W. J. Lauderdale, L. E. Halliburton, G. J. Edwards, M. P. Scripsick, P. G. Schunemann, T. M. Pollak, M. C. Ohmer, and F. K. Hopkins, Appl. Phys. Lett. 64, 1615 (1994).

282. A. Ashkin, G. D. Boyd, J. M. Dziedzic, R. G. Smith, A. A. Ballman, and [illegible], Appl. Phys. Lett. 9, 72 (1966).
283. G. D. Boyd, R. C. Miller, K. Nassau, W. L. Bond, and A. Savage, Appl. Phys. Lett. 5, 234 (1964).
284. R. B. Bylsma, P. M. Bridenbaugh, D. H. Olson, and A. M. Glass, Appl. Phys. Lett. 51, [illegible] (1987).
285. M. V. [illegible], V. [illegible], [illegible], M. [illegible], and V. I. [illegible], Ferroelectrics 22, [illegible] (1979).
286. M. Ziari, W. H. Steier, P. M. Ranon, S. Trivedi, and M. B. Klein, Appl. Phys. Lett. 60, 1052 (1992).
287. G. Pauliat and G. Roosen, J. Opt. Soc. Am. B7, 2259 (1990).
288. M. Cronin-Golomb and M. Klein, "Handbook of Optics," Vol. II, "Devices, Measurements, and Properties," Chap. 39, McGraw-Hill, Inc., New York, 1995.
289. [illegible], T. [illegible], and J. [illegible], Opt. Comm. 47, [illegible] (1983).
290. J. Feinberg and R. W. Hellwarth, Opt. Lett. 5, 519 (1980).
291. P. [illegible], H. J. von Bardeleben, and G. Roosen, [illegible] 29, 59 (1994).
292. P. Günter and J. P. Huignard (Eds.), "Photorefractive Materials and their Applications," Vol. I, Springer-Verlag, Berlin, 1988.
293. G. Pauliat and G. Roosen, Int. J. Opt. Computing 2, 271 (1991).
294. A. Chiou, [illegible], [illegible], and C. Wu, Appl. Opt. 33, 2958 (1994).
295. M. [illegible], [illegible], J. [illegible], [illegible], Y. [illegible], and [illegible], Appl. Opt. 35, [illegible] (1996).
296. D. Psaltis, D. Brady, X. Gu, and S. Lin, Nature 343, 325 (1990).
297. V. [illegible], J. Opt. Technol. 61, 827 (1994).
298. S. [illegible], [illegible], [illegible], M. [illegible], and Y. [illegible], Jpn. J. Appl. Phys. 32, Suppl. 32-3, 504 (1993).
299. K. C. [illegible], A. [illegible], and L. [illegible], Appl. Phys. Lett. 64, [illegible] (1994).
300. A. Partovi, A. Kost, E. Garmire, G. C. Valley, and M. Klein, Appl. Phys. Lett. 56, 1089 (1990).
301. J. L. [illegible] and D. T. H. Liu, Jpn. J. Appl. Phys. 29, [illegible] (1990).
302. M. Rajbenbach, J. M. Verdiell, and J. P. Huignard, Appl. Phys. Lett. 53, 541 (1988).
303. [illegible] and J. C. [illegible], Phys. Rev. B [illegible] (1991).
304. C. [illegible], H. [illegible], and L. [illegible], Chem. J. Phys. 72, [illegible] (1994).
305. J. E. Millerd, M. Ziari, and A. Partovi, in "Semiconductors and Semimetals," Vol. 58, "Nonlinear Optics in Semiconductors," p. 319 (E. Garmire and A. Kost, Eds.), Academic Press, New York, 1999.
306. D. D. Nolte, D. H. Olson, [illegible], P. M. Bridenbaugh, and A. M. Glass, Opt. Lett. 14, [illegible] (1989).
307. J. E. Millerd, S. D. Koehler, E. M. Garmire, A. Partovi, A. M. Glass, and M. B. Klein, Appl. Phys. Lett. 57, 2776 (1990).
308. J. [illegible], J. G. [illegible], A. [illegible], G. C. Valley, and M. B. Klein, Appl. Phys. Lett. 57, [illegible] (1990).
309. D. D. Nolte, D. H. Olson, and A. M. Glass, J. Appl. Phys. 68, 4111 (1990).
310. M. [illegible] and R. [illegible], International J. Nonlinear Optical Physics 3, 223 (1994).
311. M. [illegible] and P. [illegible], International J. Nonlinear Optical Physics 3, [illegible] (1994).
312. M. Wolffer and P. Gravey, Opt. Comm. 107, 115 (1994).
313. C. [illegible], S. [illegible], P. [illegible], [illegible], and G. [illegible], J. Opt. Soc. Am. B11, [illegible] (1994).
314. K. [illegible], Y. [illegible], T. [illegible], R. [illegible], M. [illegible], M. [illegible] and [illegible], Opt. Lett. 13, [illegible] (1988).
315. M. J. van [illegible], J. C. Launay, and V. [illegible], Appl. Phys. Lett. 64, [illegible] (1993).
316. Y. Belaud, P. Delaye, J. C. Launay, and G. Roosen, Opt. Comm. 105, 204 (1994).
317. J. C. Launay, V. Mazoyer, M. Tapiero, J. P. Zielinger, Z. Guellil, Ph. Delaye, and G. Roosen, Appl. Phys. A55, 33 (1992).

318. J. Y. Moison, N. Wolffer, O. [illegible], P. [illegible], G. Marcel, A. Aoddia, B. [illegible], Y. [illegible], and R. Triboulet, *J. Opt. Soc. Am.* B11, 1[illegible] (1994).
319. A. Ferrand, J. Milliard, H. [illegible] Gonzales, M. Zhao, W. H. [illegible], A. E. Thiesen, and M. E. [illegible], *Appl. Phys. Lett.* 57, [illegible] (1990).
320. B. [illegible], A. Aoddia, M. [illegible], A. [illegible], Y. [illegible], R. Triboulet, G. [illegible], G. [illegible], B. Chevreuil, M. C. [illegible], J. M. [illegible], M. [illegible], P. [illegible], J. Y. Moison, P. Georges, N. Wolffer, and G. [illegible], *J. Cryst. Growth* 13[illegible], 344 (1994).
321. R. M. [illegible], M. Zhao, and B. [illegible], *Phys. Rev.* B49, [illegible] (1994).
322. J. C. Launay, V. [illegible], M. [illegible], J. P. [illegible], E. [illegible], Ph. Delaye, and G. Roosen, *Appl. Phys.* A55, 33 (1992).
323. J. Y. Moison, N. Wolffer, O. [illegible], P. Georges, G. Marcel, A. Aoddia, B. [illegible], Y. [illegible], and R. Triboulet, *J. Opt. Soc. Am.* B11, 1[illegible] (1994).
324. J. Y. Moison, P. Georges, N. Wolffer, O. [illegible], R. Triboulet, and A. Aoddia, "[illegible] on Photorefractive Materials, Effects and Devices," [illegible] 93, [illegible] (1993).
325. Y. [illegible], P. Delaye, J. C. Launay, and G. Roosen, *Opt. Commun.* [illegible] 204 (1994).
326. G. Marcel, J. Y. Moison, E. [illegible], M. [illegible], B. [illegible], N. Wolffer, P. Georges, A. Aoddia, B. [illegible], Y. [illegible], R. Triboulet, M. C. [illegible], M. [illegible], J. M. [illegible], P. [illegible], G. [illegible], A. [illegible], and G. [illegible], *J. Crystal Growth* 1[illegible], 2[illegible] (1995).
327. G. [illegible], B. [illegible], R. [illegible], [illegible], A. [illegible], and D. [illegible], *Opt. Lett.* 16, [illegible] (1991).
328. R. [illegible], R. M. [illegible], E. D. [illegible], J. G. [illegible], B. [illegible], R. [illegible], R. Meigen, A. Burger, and B. [illegible], *J. Electron. Mater.* 2[illegible], 669 (1997).
329. M. [illegible], W. H. [illegible], J. Milliard, J. [illegible], G. [illegible], E. [illegible], and B. B. Thiesen, "[illegible] Conference on Nonlinear Optical Materials, Fundamentals and Applications," [illegible], 1994.
330. R. H. Meigen, M. [illegible], E. [illegible], K.-T. [illegible], B. [illegible], E. L. [illegible], and A. Burger, "Proceedings of the MRS 1997 Spring Meeting," Vol. 4[illegible], [illegible] 1997.
331. W. H. [illegible], J. [illegible], and M. [illegible], *Appl. Phys. Lett.* 53, [illegible] (1988).
332. L. W. [illegible] and T. F. Boggess, *Prog. Quant. Electr.* 17, 2[illegible] (1993).
333. T. Y. Chang, [illegible], J. H. Hong, and M. [illegible], *Mat. Res. Soc. Symp. Proc.* 3[illegible], 6[illegible] (1994).
334. [illegible], [illegible], and [illegible], *Mat. Res. Soc. Symp. Proc.* 4[illegible], 1[illegible] (199[illegible]).
335. T. F. [illegible], *J. [illegible]* 4, [illegible] (1995).
336. J. B. [illegible], [illegible], D. W. [illegible], and T. C. [illegible], *Phys. Rev. Lett.* 19, 1[illegible] (19[illegible]).
337. A. M. [illegible] and K. K. Chang, *Appl. Phys. Lett.* 55, [illegible] (19[illegible]).
338. V. V. [illegible], V. A. [illegible], D. N. [illegible], and A. N. [illegible], *Sov. Phys. JETP* 2[illegible], 41[illegible] (19[illegible]).
339. L. W. Tutt and T. F. Boggess, *Prog. Quant. Electr.* 17, 299 (1993).
340. T. F. Boggess, S. C. Moss, I. W. Boyd, and A. L. Smirl, *Opt. Lett.* 9, 291 (1984).
341. T. F. Boggess, A. L. Smirl, S. C. Moss, I. W. Boyd, and E. W. Van Stryland, *IEEE J. Quantum Electron.* 21, [illegible] (1985).
342. A. A. Said, M. Sheik-Bahae, D. J. Hagan, [illegible], Y. Y. Wu, J. Young, T. H. Wei, and E. W. Van Stryland, *Proc. SPIE* 1307, 404 (1990).
343. P. F. [illegible], *J. Chem. Soc. Am.* [illegible], 125 (19[illegible]).
344. [illegible] and P. R. [illegible], *Optics Lett.* 13, [illegible] (19[illegible]).
345. G. [illegible] and E.-J. [illegible], *Z. Naturforsch.* 73 a, [illegible]–1[illegible] (19[illegible]).
346. B. H. T. [illegible], L. D. [illegible], K. I. [illegible], P. O. [illegible], R. J. [illegible], R. A. [illegible], W. F. Krupke, and A. Burger, "OSA TOPS on Advanced Solid-State Lasers," Vol. 1, pp. 1[illegible]–1[illegible] (Stephen A. Payne and Clifford Pollock, Eds.), Optical Society of America, Washington, DC 1996.
347. [illegible], [illegible], J. A. [illegible], B. J. [illegible], R. J. [illegible], S. A. Payne, and W. F. Krupke, in "OSA Trends in Optics and Photonics," Vol. [illegible], "Advanced Solid State Lasers," pp. [illegible]–21[illegible] (C. R. Pollock and W. R. Bosenberg, Eds.), Optical Society of America, Washington, DC 1997.

348. J. McKay, K. L. Schepler, and G. Catella, "OSA TOPS," Vol. 26, "Advanced Solid-State Lasers," pp. 420–425 (Martin M. Fejer, Hagop Injeyan, and Ursula Keller, Eds.), Optical Society of America, Washington, DC, 1999.
349. D. Hömmerich, X. Wu, V. R. Davis, S. R. Trivedi, K. Grasza, R. J. Chen, and S. [illegible], Opt. Lett. 22, 1180 (1997).
350. G. J. Wagner, T. J. Carrig, R. H. Page, K. I. Schaffers, J.-O. Ndap, X. Ma, and A. Burger, Opt. Lett. 24(1), 19 (1999).
351. M. C. Ohmer and R. Pandey, MRS Bulletin 23, 16 (1998).
352. J. L. Shay and J. H. Wernick, "Ternary Chalcopyrite Semiconductors: Growth, Electronic Properties, and Applications," Pergamon Press, New York, 1975.
353. R. P. Dunn, [illegible] J. Nonlinear Opt. Phys. 1, 639 (1992); in "Tunable Lasers Handbook," Chapter 7, pp. 195–346 (F. J. Duarte, Ed.), Academic Press, New York, 1995.
354. P. G. Schunemann, K. L. Schepler, and P. A. Budni, MRS Bulletin 23, 45 (1998).
355. D. W. Fischer and M. C. Ohmer, J. Appl. Phys. 81, 425 (1997).
356. P. G. Schunemann and T. M. Pollak, MRS Bulletin 23, 23 (1998).
357. N. C. Giles and L. E. Halliburton, MRS Bulletin 23, 37 (1998).
358. R. Pandey, M. C. Ohmer, A. Costales, and J. M. Recio, Mat. Res. Soc. Symp. Proc. 484, 585 (1998).
359. S. H. Baiman, [illegible], MRS Bulletin 23, 41 (1998).
360. P. A. Budni, L. A. Pomeranz, M. L. Lemons, P. G. Schunemann, T. M. Pollak, and E. P. Chicklis, in "OSA Trends in Optics and Photonics," Vol. 19, "Advanced Solid State Lasers," pp. 226–229 (W. R. Bosenberg and M. M. Fejer, Eds.), Optical Society of America, Washington, DC, 1998.
361. A. G. Jackson, M. C. Ohmer, and S. R. LeClair, Infrared Physics & Technology 38, 233 (1997).
362. G. D. Boyd, H. Kasper, J. H. McFee, and J. H. Wernick, IEEE J. Quantum Electron. 8, 419 (1972).
363. P. G. Schunemann, "Conference on Lasers and Electro-Optics and Laser Science (QELS)—Technical Digest Series Proceedings of the 1996 IEEE Quantum Electronics and Laser Science Conference," QELS, Jun 2–7 1996, v 9 1996 Anaheim, CA, 1996. Sponsored by IEEE, Piscataway, NJ, USA, p. 56.
364. R. Dasbach and K. Kunz, Mat. Res. Soc. Symp. Proc. 484, 475 (1998).
365. M. L. [illegible] and C. [illegible], Mat. Lett. 12, 39 (1991).
366. G. J. Brown, M. C. Ohmer, and P. G. Schunemann, Mat. Res. Soc. Symp. Proc. 484, 531 (1998).
367. G. Lebrun, A. E. Chorge, A. M. [illegible], R. E. Pease, A. [illegible], and M. R. [illegible], J. Cryst. Growth 208, 319 (2000).
368. H. Kildal and G. W. Iseler, Appl. Opt. 15, 3062 (1976).
369. G. W. Iseler, H. Kildal, and N. Menyuk, J. Electron. Mater. 7, 737 (1978).
370. P. G. Schunemann, in "Conference on Lasers and Electro-Optics," 1999, "OSA Technical Digest Ser.," Vol. 8, p. 255, Optical Society of America, Washington, DC, 1999.
371. R. Triboulet and R. Rose, Mat. Res. Soc. Symp. Proc. 484, 479 (1998).
372. R. L. Byer, in "Treatise in Quantum Electronics," p. 587 (H. Rabin and C. L. Tang, Eds.), Academic Press, New York, 1975.
373. G. C. Catella and D. Burlage, MRS Bulletin 23, 28 (1998).
374. J.-M. Spaeth, J. R. Niklas, and R. H. Bartram, "Structural Analysis of Point Defects in Solids," Springer-Verlag, Berlin, 1992.
375. W. Ruderman, J. Maffetone, D. R. Zelman, and D. M. Poirier, Mat. Res. Soc. Symp. Proc. 484, 519 (1998).
376. B. Halsley and H. Lu, Opt. Commun. 171, 171 (1999).
377. G. C. Bhar, S. Das, D. Chatterjee, P. K. Datta, and Yu. M. Andreev, Appl. Phys. Lett. 63, 1316 (1993).
378. G. C. Bhar, S. Das, D. V. Satyanarayan, P. K. Datta, U. Nundy, and Yu. M. Andreev, Opt. Lett. 20, 2057 (1995).

379. C. [illegible], I. [illegible], A. [illegible], F. [illegible], and M. [illegible], *J. [illegible] Sci.* 31, 3[illegible] (199[illegible]).

380. M. C. [illegible], J. T. [illegible], [illegible], A. W. [illegible], S. M. [illegible], J. D. Wolf, F. C. [illegible]-[illegible], and T. M. [illegible], *J. Appl. Phys.* [illegible] (19[illegible]).

381. D. M. [illegible], G. A. [illegible], and R. T. [illegible], "OSA Proceedings on Advanced Solid-State Lasers," vol. [illegible], pp. [illegible] (B. H. T. Chai and S. A. Payne, Eds.), Optical Society of America, Washington, DC, 1995.

382. D. S. [illegible] and R. A. Chipman, *Appl. Opt.* [illegible] (199[illegible]).

383. T. [illegible], [illegible], [illegible], P. [illegible], J. A. [illegible], and [illegible], "OSA [illegible]," vol. 1[illegible], "Advanced Solid-State Lasers," p. [illegible] (Clifford R. Pollock and Walter R. Bosenberg, Eds.), Optical Society of America, Washington, DC, 199[illegible].

384. [illegible] A. [illegible], L. A. [illegible], A. M. [illegible], A. D. [illegible], [illegible], and V. V. [illegible], *JETP Lett.* [illegible] (19[illegible]).

385. K. L. [illegible] and V. [illegible], *Optics Comm.* 11[illegible], [illegible] (19[illegible]).

386. K. L. [illegible] and V. [illegible], *Optics Comm.* 1[illegible], [illegible] (19[illegible]).

387. N. [illegible], *Progr. Crystal Growth Characterization* [illegible] (19[illegible]).

388. G. [illegible] and J. L. [illegible], *J. Phys. Chem. Solids* [illegible] (19[illegible]).

389. R. H. [illegible] and [illegible], *Phys. Rev.* [illegible] (19[illegible]).

390. W. T. [illegible], *J. Phys. C: Solid State Phys.* [illegible] (19[illegible]).

391. C. D. [illegible] and A. [illegible], *J. Crystal Growth* [illegible] (19[illegible]).

392. E. [illegible] and M. [illegible], *Philos. Mag.* [illegible] (19[illegible]).

393. N. B. Singh, T. [illegible], V. [illegible], D. E. [illegible], N. C. [illegible], R. H. Hopkins, and [illegible], *J. Crystal Growth* [illegible] (19[illegible]).

394. N. B. Singh, T. [illegible], R. H. Hopkins, K. C. [illegible], R. [illegible], and [illegible], *Progress in Crystal Growth and Characterization* [illegible] (19[illegible]).

395. N. C. [illegible], B. [illegible], N. B. Singh, [illegible], M. [illegible], R. H. Hopkins, R. [illegible], and [illegible], *Mat. Res. Soc. Symp. Proc.* [illegible] (19[illegible]).

396. A. [illegible], S. [illegible], W. [illegible], D. I. [illegible], M. [illegible], A. [illegible], R. L. [illegible], and V. V. [illegible], *Optics Communications* [illegible] (19[illegible]).

397. M. Sparks, *J. Appl. Phys.* [illegible] (19[illegible]).

398. [illegible] and P. [illegible], *J. Electron. Mater.* [illegible] (19[illegible]).

399. [illegible] and R. A. [illegible], *J. Appl. Phys.* [illegible] (19[illegible]).

400. [illegible], [illegible], [illegible], F. C. [illegible], and M. [illegible], *Appl. Opt.* [illegible] (19[illegible]).

401. G. [illegible] and [illegible], *J. American Ceramic Society* [illegible] (19[illegible]).

402. [illegible] T. [illegible], *J. Electronic Materials* [illegible] (19[illegible]).

403. A. W. [illegible], M. [illegible], [illegible], and C. L. [illegible], *Appl. Opt.* [illegible] (19[illegible]).

404. M. Sparks, Theory of Multiphonon Infrared Absorption. Presented at Air Force Laser Window Conference, [illegible], MA, 1972.

405. A. L. [illegible], J. E. [illegible], [illegible], and [illegible], *Mat. Res. Bull.* [illegible] (19[illegible]).

406. [illegible] and [illegible], *J. Appl. Phys.* [illegible] (19[illegible]).

407. M. Sparks, *J. Appl. Phys.* [illegible] (19[illegible]).

408. M. [illegible] and [illegible], *International J. Nonlinear Optical Physics* [illegible] (199[illegible]).

409. M. [illegible] and [illegible], *International J. Nonlinear Optical Physics* [illegible] (199[illegible]).

410. J. Y. [illegible], P. [illegible], N. [illegible], [illegible], [illegible], Y. [illegible], [illegible], M. C. [illegible], [illegible], [illegible], and F. [illegible], *Opt. Mat.* [illegible] (199[illegible]).

411. W. M. Higgins, R. M. [illegible], K. J. [illegible], M. B. [illegible], T. M. [illegible], and D. J. [illegible], The [illegible] on the properties of [illegible] Phosphide. Presented at the [illegible] Phosphide and Related Materials (IPRM) Conference, [illegible], May 199[illegible].

412. M. Sugre and K. Tada, *Japan J. Appl. Phys.* 15, 421 (1976).
413. A. G. Debell, E. L. Dereniak, J. Harvey, J. Nissley, J. Palmer, A. Selvarajan, and W. L. Wolfe, *Appl. Opt.* 18, 3114 (1979).
414. I. P. Kaminow, in "Handbook of Laser Science and Technology," Vol. IV, "Optical Materials, Part II: Properties," p. 253 (M. J. Weber, Ed.), CRC Press, Boca Raton, 1986.